

Report



LFCS Review report – Structure and mooring response

Author(s)

Bernt Leira, Marit Kvittem, Hagbart Skage Alsos, Ivar Fylling



SINTEF Ocean AS

Address:
Postboks 4760 Torgarden
NO-7465 Trondheim
NORWAY

Switchboard: +47 46415000

Enterprise /VAT No:
NO 937 357 370 MVA

Report

LFCS Review report – Structure and mooring response

REPORT NO.	PROJECT NO.	VERSION	DATE
OC2018 A-073-WP3/WP4	302001772-5	1.0	2019-04-29

KEYWORDS:Large floating bridges;
Structural response;
Mooring response**AUTHOR(S)**

Bernt Leira, Marit Kvittem, Hagbart Skage Alsos, Ivar Fylling

CLIENT(S)

KPN-project LFCS Industry partners and Norwegian Research Council (NRC)

CLIENT'S REF.**NUMBER OF PAGES/APPENDICES:**

66

CLASSIFICATION

Unrestricted

CLASSIFICATION THIS PAGE

Unrestricted

ISBN

978-82-7174-383-3

ABSTRACT

A review is performed on structural and mooring response analysis work in relation to Large Floating Coastal Structures and the planning of long floating bridges across fjords. The review contains observations on global response methodology, environmental loading and interactions, mooring design, measurements and validation, and finally design criteria and limit states. The basis for the review is mentioned but described in detail in the LFCS Introduction and Summary report (OC2018 F-073-WP0). Tables of identified gaps are presented along with recommendations for further work.

**PREPARED BY**

Bernt Leira

CHECKED BY

Halvor Lie

APPROVED BY

Vegard Aksnes

Dokumentet har gjennomgått SINTEFs godkjenningsprosedyre og er sikret digitalt

PROJECT NO.
302001772-5REPORT NO.
OC2018 A-073-WP3/WP4VERSION
1.0

Page 1 of 66

Document History

VERSION	DATE	VERSION DESCRIPTION
Draft	2018-09-15	Draft version for Workshop (Sept.24-25) comments

1.0	2019-04-29	Final version
-----	------------	---------------

Table of Contents

1	Introduction	5
1.1	General.....	5
1.2	Description of Document.....	5
1.3	Scope of Work – WP3, WP4 Review	6
2	Summary and Conclusions	7
2.1	Summary of review – WP3 and WP4	7
2.2	Identified Knowledge Gaps	7
2.3	Identified Software Functionality Gaps	8
2.4	Recommendation for Further Work	8
3	Review Basis	10
4	Observations and Review	11
4.1	Observations from structural response analyses	11
4.1.1	Critical responses/observation points	11
4.1.2	Structural parameter studies.....	11
4.1.3	Modal analysis and contribution from modes to critical response	13
4.2	Global response analysis methodology	18
4.2.1	Hand calculations.....	18
4.2.2	Numerical methods and models.....	20
4.2.3	Boundary conditions.....	23
4.2.4	Frequency Domain Solvers (linear).....	24
4.2.5	Time domain solvers (linear/non-linear)	27
4.2.6	Capabilities and performance of applied software packages	27
4.3	Wave loads.....	28
4.3.1	First order wave loads	28
4.3.2	Wave spectrum (wind sea, swell)	28
4.3.3	Wave spreading	29
4.3.4	Inhomogeneous wave conditions across the span.....	29
4.3.5	Hydrodynamic interaction between pontoons	31
4.3.6	Second order wave loads.....	32
4.3.7	Waves from Passing Vessels	33
4.4	Wind Loads.....	33
4.4.1	Aerodynamic Loads	33
4.4.2	Vortex Induced Vibrations (VIV) and Aerodynamic Instabilities	34
4.4.3	Effect of Wind Spectrum.....	35
4.4.4	Inhomogeneous Wind Field Across the Span	37
4.4.5	Effect of Wave on Vertical Turbulence	37

4.5	Current Loads.....	38
4.6	Other Loads.....	38
4.6.1	Permanent loads.....	39
4.6.2	Water level variations.....	39
4.6.3	Temperature loads	39
4.6.4	Traffic loads	40
4.7	Effects of interaction between loads.....	41
4.8	Mooring design	43
4.8.1	Description of straight bridge of Bjørnafjorden	43
4.8.2	Uncertainties	44
4.9	Measurements and validation of response calculations	46
4.9.1	Wave response	46
4.9.2	Wind response.....	46
4.10	Design criteria, limit states and response.....	47
4.10.1	Design criteria and limit states	47
4.10.2	Characteristic load calculation.....	49
4.10.3	Load combination	50
4.10.4	Design principles and critical response components	54
4.10.5	Observations from design checks.....	55
5	Identification of Gaps	56
5.1	Uncertainties and gaps in Design Methods (related directly to WP3 and WP4).....	56
5.2	Uncertainties and Gaps Related to Environmental Description (WP1).....	57
5.3	Uncertainties and Gaps Related to Loads (WP2).....	57
5.4	Uncertainties and Gaps Related to Model Tests (WP5)	58
5.5	Limitations in Software	58
6	Recommendations.....	59
6.1	Work package 3 and 4 connections to other work packages	59
6.2	Scope for Methodology Development for WP3 and WP4	59
6.3	Scope for Case Studies for WP3 and WP4 (models, generic, etc.)	60
6.4	Scope for software improvement.....	61
7	References	62
7.1	General.....	62
7.2	Bjørnafjorden Crossing.....	62
7.3	Sulafjorden Crossing	63
7.4	Lysefjorden.....	63
7.5	Other bridges	63
Appendix A	Bridge concepts; some examples.....	65

[List appendices here]

1 Introduction

1.1 General

The KPN project "Design and verification of Large Floating Coastal Structures" (LFCS) started with a kick-off of Nov.30, 2017, with a planned duration to summer of 2021. The project was established by SINTEF Ocean and NTNU with the support of the Norwegian Research Council, the Norwegian Public Road Administration, Hydro ASA, Multiconsult AS, SWECO AS, and LMG Marin AS



Compared with well-established methods in ocean engineering, the following critical issues are initially identified for the analysis of large floating coastal structures,

- varying bathymetry and inhomogeneous environmental conditions over the extension of the structure
- inhomogeneous environmental loads over the structure,
- hydroelasticity of large floating coastal structures under inhomogeneous conditions,
- mooring and station-keeping of large flexible floating structures,
- modelling of hydroelastic effects in combinations with articulated/elastic interconnections between structural parts.

One objective of the present project is to improve the understanding of each of these separate topics, and then to provide input to a consistent procedure for design and verification of large floating coastal structures. The project is then organized in work packages according to the identified topics above:

- WP1 - Environmental description
- WP2 - Environmental loads
- WP3 - Structural response
- WP4 - Mooring and positioning
- WP5 - Model testing

In addition, the LFCS administrative tasks have been organized in a work package WP0.

Review phase:

The first phase of the project is devoted to a review of work already performed for relevant existing structures, for conceptual studies performed for potential crossings as well as additional work on measurements, modelling, simulations related to coastal areas which in all comprises the state of the art. This also included a 2-day workshop on March 7-8 with emphasis on environmental description, modelling and loads, and structural response based on presentations from the LFCS industry partners and specially invited external presenters.

1.2 Description of Document

This document presents a review of state of the art with respect to methods, software and gaps for the response of large floating structures subjected to inhomogeneous environmental loads. Focus is placed on topics addressed by work packages WP3 and WP4 which are naturally linked. Work package 3 deals with

the analysis and response of large floating structure subjected to inhomogeneous loads. WP 4 addresses the response on and from mooring lines on the large floating structure.

1.3 Scope of Work – WP3, WP4 Review

The objective for the review (WP3, WP4) is to generate the literature review basis and perform a review of methods, analyses and responses for large floating structures subjected to inhomogeneous environmental loads.

The review basis is described in the Introductory document – LFCS Review draft report – Introduction and Summary, OC2018 F-073-WP0. A brief and general overview is:

- design documents for the Bjørnafjorden crossing – conceptual design phase III,
- public documents from previous conceptual design phases for Bjørnafjorden
- public documents from feasibility studies for other fjords and potential crossings, such as Sognefjord and Sulafjord
- deliveries from the E39 ferry-free PhD programme,
- available documents from the design and testing of existing floating bridges
- conference proceedings
- articles published in academic journals.

The review is performed to survey and outline the state of art within analysis tools, analysis methodologies, applied loads and calculated responses observed for large floating structures. This is then applied to identify gaps in existing methods and their importance for response, load effects, respective failure modes and limit states. The proposed gaps and recommended actions will then form a basis for decision in the LFCS-project on further work related to the work packages WP3 and WP4.

2 Summary and Conclusions

2.1 Summary of review – WP3 and WP4

Several uncertainties and knowledge gaps concerning structure and mooring response were identified in the review process. These gaps relate to:

- uncertainties in environment description
- uncertainties in load models,
- statistical uncertainty,
- modelling method uncertainty and
- software functionality.

The main knowledge gaps identified in this work package are listed in Section 2.2, and software functionality gaps are listed in Section 2.3. Recommended further work is listed in Section 2.4. Gaps and recommendations that are closely linked to the other work packages are listed in Sections 5 and 6. The gaps are not listed in a prioritized order.

2.2 Identified Knowledge Gaps

Table 1 Identified knowledge gaps

Knowledge gap	Actions required to close gap (sensitivity studies, method development, numerical tool development, model tests, full scale measurements)
Correlation basis for combination of environmental loads in calculation of characteristic response (section forces)	Reliability analysis
Interaction effects between wind, wave and current loads	Numerical sensitivity studies
Mooring system functional requirements beyond mandatory requirements, i.e. to reduce response	Discussion of the anchor system's role in ensuring satisfactory bridge response
Mooring system damping effects on response	Numerical sensitivity studies and hydrodynamic model tests
Mooring system influence on mode shapes and dynamic behaviour of the bridge	Numerical sensitivity studies
Response after line failure(s) possible implication on design	Study on mooring line system effects
Complex numerical models for response analysis	Establish best practice for modelling of floating bridges
Uncertainty in extreme value calculation [$X_{\max} = k \cdot \sigma$, where k is a response gust factor] <ul style="list-style-type: none"> • Gaussian • Non-Gaussian 	Uncertainty analysis and assessment of necessary simulation length and number of random realizations.
Characteristic environmental condition; wind (10 min.), wave (3 hours), current - to 1 hour response timeseries	1): Environmental condition: compare averages based on gust (3 sec), 10 min wind, 60 min wind 2): Perform response analysis to show the effects.
Criteria for occurrence of global dynamic buckling (of curved bridges)	Development of engineering models (<i>Outside of scope for LFCS.</i>)

Knowledge gap	Actions required to close gap (sensitivity studies, method development, numerical tool development, model tests, full scale measurements)
Shear lag effect in global response analysis	Incorporation of shear lag effect in global analysis; <ul style="list-style-type: none"> • Redesign • Account for shear lag <i>(Outside of scope for LFCS.)</i>
Mooring system design rules and safety factors for 100-year design life	Reliability analysis <i>(Outside of scope for LFCS.)</i>

2.3 Identified Software Functionality Gaps

Table 2 Identified software functionality gaps

Knowledge gap	Actions required to close gap (sensitivity studies, method development, numerical tool development, model tests, full scale measurements)
Numerical inhomogeneous wave field description	Implement in SIMO/RIFLEX (stand-alone tool to pre-generate wave forces or as wave field description in the code)
Inhomogeneous wind field in SIMO/RIFLEX	Develop turbulence generator with inhomogeneous conditions
Wind field with adaptive grid for long bridges	Develop grid generator
Frequency-dependent aerodynamic properties in time domain simulations	Implement state-space model for wind loads. Input from already performed wind tunnel tests for the testing of the state-space modelling. <i>(Outside of scope for LFCS to perform new wind tunnel tests.)</i>
Numerical models for response analysis are large and complex	Benchmarking studies, instruction manuals (for modelling [structure, mass, damping], execution of analysis, sample size, etc.) specially written for floating bridges
Hydrodynamic interaction matrices in global response analysis (numerical tool gap)	Implement in SIMO/RIFLEX (for required number of pontoons according to interaction effect (any software limitation?))
Linear analysis in hydrodynamic analysis solvers (SIMO/RIFLEX)	Implement linear solvers and eigenvalue solvers considering frequency dependent added mass and damping
Frequency domain solver for fatigue analysis of floating bridges (SIMO/RIFLEX)	Implementation of frequency domain solver in SIMO/RIFLEX

2.4 Recommendation for Further Work

There are several topics that should be studied in more detail as part of future work within the present project. In general, quantification of various sources of uncertainty and the resulting effects on the static and dynamic structural response levels is required.

One important aspect of this is the quantification of uncertainties related to methods for representation of inhomogeneous wave and wind conditions at various levels of approximation. Furthermore, detailed studies of uncertainties related to methods for propagation analysis of characteristic environmental parameters from the open ocean to a given local site are required. As part of this, comparison of numerical propagation models with results from site measurements (e.g. in the Bjørnafjord) represents a key activity.

At the other end, the effect of these uncertainties on the computed static and dynamic structural response of relevant bridge concepts must be addressed. This applies in particular to identification of situations where inhomogeneous load processes may lead to response amplification as compared to homogeneous conditions.

Within such a context, computation of long-term response statistics is of key importance. The likelihood of possible response amplification phenomena and resulting effects on extreme values as well as fatigue damage accumulation can then be properly assessed.

Recommended topics for further work within WP3 and WP4 are listed in the table below.

Table 3 Recommended topics for further work within WP3 and WP4

Item	Description
Response to inhomogeneous waves	Assess response to inhomogeneous wave field. Compare with homogenous waves.
Response to inhomogeneous wind	Assess response to inhomogeneous wind field. Compare with homogenous wind.
Combination of environmental load effects	Compare methods for combination of environmental load effects from different environmental loads as well as combination of different cross-section forces; static, dynamic, extreme.
Estimating uncertainty in extreme response predictions	Calculate long term response characteristics of response to inhomogeneous conditions and compare with results from simplified methods. Compare results from various simplified extreme response estimation methods toward long-term extreme response.
Model truncation study	Compare a numerical model of the whole bridge length to a model with reduced length; investigate the limitations of the reduced length model to be used in hydrodynamic model tests. Find reasonable boundary conditions for the reduced model tests.
Effect of limited number of actuators	For model tests, investigate the implications of reduced number of degrees of freedom for actuation of wind loads in hydrodynamic model tests.
Interaction effect between wave and wind loads	Investigate the implications of superposition of wind and wave load effects.
Hydrodynamic interaction between pontoons	Effect of diffraction and added mass considering interaction between pontoons on full model in short-crested irregular sea. Compare to model with no interaction.
Validity of Newman's approximation	Compare slow drift response calculated by Newman's approximation to response with full QTFs calculated for a flexible structure.
Tuning of numerical model to hydrodynamic experiments	Full scale numerical model with hydrodynamic coefficients tuned to model tests.
Mooring system damping	Numerical sensitivity study of mooring system damping

Item	Description
Buffeting theory vs. quasi-steady non-linear theory	Compare the responses for two different approaches.
Sensitivity to low frequency content in wind spectrum	Simulation of full bridge model with wind loads from spectrum based on measurements.

3 Review Basis

The review basis is described in the Introductory document – LFCS Review draft report – Introduction and Summary, OC2018 F-073-WP0. A brief and general overview is:

- Design codes
- Conceptual design documents for the Bjørnafjorden crossing, phases I to III
- Feasibility studies for Sognefjord and Sulafjord
- Design, studies and model tests performed for Bergsøysundet floating bridge and Nordhordland floating bridge
- Deliveries from the E39 ferry-free PhD programme,
- Conference proceedings
- Articles published in academic journals.

4 Observations and Review

The review covers design summaries from the three different bridge concepts for the Bjørnafjorden crossing: Cable-stayed, straight, moored bridge, cable-stayed, end-anchored, curved bridge and TLP straight suspension bridge. In addition, journal and conference papers that were considered relevant for long, floating bridge research have been included in the review.

4.1 Observations from structural response analyses

4.1.1 Critical responses/observation points

Bridge girder (given along the length)

- Cross section global forces (in particular weak and strong axis bending moments) (ULS, FLS)
- Global and local displacements and accelerations (SLS)

Pontoons

- Rigid body translations and rotations
- Rigid body accelerations

Mooring lines

- Axial force
- Fairlead displacement

Cables (stay cables or suspension)

- Axial force

Towers

- Tower leg cross section forces
- Tendon axial force (for TLP towers)

4.1.2 Structural parameter studies

The summary report for the end-anchored curved bridge [6] concludes on sensitivity studies performed as part of the design work with this concept. The findings are summarised below, supplemented with observations for the straight bridge [5] and [20]. The observations are considered relevant for both concept types, except for parameters concerning curvature and mooring.

Bridge length	A longer bridge increases the natural periods and thus the wind induced response. This effect can be reduced by lowering the height of the bridge girder.
Bridge curvature	Larger radius gives larger axial load, influences stiffness, but no significant effect on response.
Curve direction	Curve in the direction of the wind is positive for buckling due to mean wind.

Bridge girder cross section	Reducing the bridge girder box height has a large effect on reducing the wind drag. The stiffness of the bridge girder has some influence on the roll stability of the bridge [5].
Pontoon spacing	The most important parameter for the load effect from permanent loads. 100 m was chosen based on steel quantity estimates for various span lengths. Smaller spacing means smaller stresses in the girder from traffic and permanent loads. A similar analysis of overall steel weight was performed for the straight bridge, where 125 m pontoon spacing was chosen [5].
Pontoon material	Due to the weight of concrete, the pontoons need to be larger than steel pontoons to achieve the necessary buoyancy. In turn, this leads to larger wave loads, and larger loads in the bridge girder.
Pontoon shape	Letting the length of the pontoons be equal to the critical wave length, means cancellation of the horizontal Froude-Krylov wave force. The shape of the pontoon can be used to ensure phase distribution along the bridge. For the straight bridge, this was obtained with a diamond shape pontoon. Pontoons with small water plane areas get less wave excitation.
Pontoon flange	Pontoon flanges can be used to increase the added mass in heave and thus regulate the natural periods but can also decrease damping and increase roll motion. Possible increasing in wave loads.
Mass	Increase in pontoon mass leads to increased wind, wind generated wave and swell response due to longer eigen-periods.
Restoring stiffness pontoons	Increased restoring stiffness in heave leads to larger wind wave and tidal variation response. Increasing the heave, pitch and roll restoring is beneficial for pontoon traffic response but increases the bridge girder moment. The roll stability of the bridge depends in the pontoon restoring stiffness [5] from hydrostatic forces and rotational stiffness of the bridge girder.
Bridge girder stiffness	Reducing the bridge girder stiffness, increases the wind response due to longer eigen-periods. With increased stiffness, the moments due to wind driven waves, swell and tidal variations may experience small increases.

4.1.3 Modal analysis and contribution from modes to critical response

Design reports for the three Bjørnafjorden crossing concepts report the eigenperiods and eigenmodes of the structures. These are shown in Figures 1-3 below, together with excitation load ranges for wind, first- and second order wind wave forces and swell waves. The excitation load ranges shown are based on wind and wave data reported in the Bjørnafjorden Design Basis [3], and are set to:

- Wave periods: 1.5 – 7.1 s
- Wind periods: 8 – 200 s
- Swell waves: 10 – 19 s

Figures 1-3 sort the modes by dominating mode, but it should be noted that some of these modes have strong coupling, e.g. between lateral and torsional displacement.

For all concepts, there are several eigen frequencies within the wind or wave excitation range. It is therefore difficult to design the structure to avoid excitation frequencies. However, even if a mode is within the excitation frequency range, it does not necessarily mean that there will be significant dynamic amplification of that mode. In the lowest part of the range, wave heights and wind speeds may be so low that loads are negligible compared to static loads, and not even relevant for consideration in ultimate limit states. Also, the response may not contribute to the critical response. Thus, in addition to Figures 1-3, a summary of the reported contribution from the different modes to critical responses is given.

The following observations were made in the wind- and wave response analysis for the end-anchored curved bridge[6] and the side anchored straight bridge [5]:

- The two lowest eigen-periods in the lateral direction for the end anchored bridge are higher than the side-anchored bridge, due to the stiffness of the mooring system of the latter.
- Wind loads are the dominating contribution to strong axis bending of the girder for both the curved and the straight bridge. The 5 lowest eigenmodes could be observed in the analyses.
- Wind sea dominated the weak axis response of the bridge girder through exciting pontoon heave motion. Multiple eigenmodes were triggered and complex resonant behaviour was observed.
- Wave induced heave motion couples with rotational modes of the bridge.
- The lowest mode in torsion give largest rotations around the transition between the cable stayed part and the low part of the bridge.
- For lateral loads, the wind induced response seems to contribute to alleviate wave induced lateral response (straight bridge).
- Many of the critical responses, e.g. maximum bridge girder weak axis moment and torsion, can be found in the transition between the high and the low bridge.
- Swell triggered horizontal modes between 12-25 s, but the contribution was small compared to wind response (curved bridge observation).
- Third party independent load analysis resulted in higher loads than obtained by the designer for the straight bridge

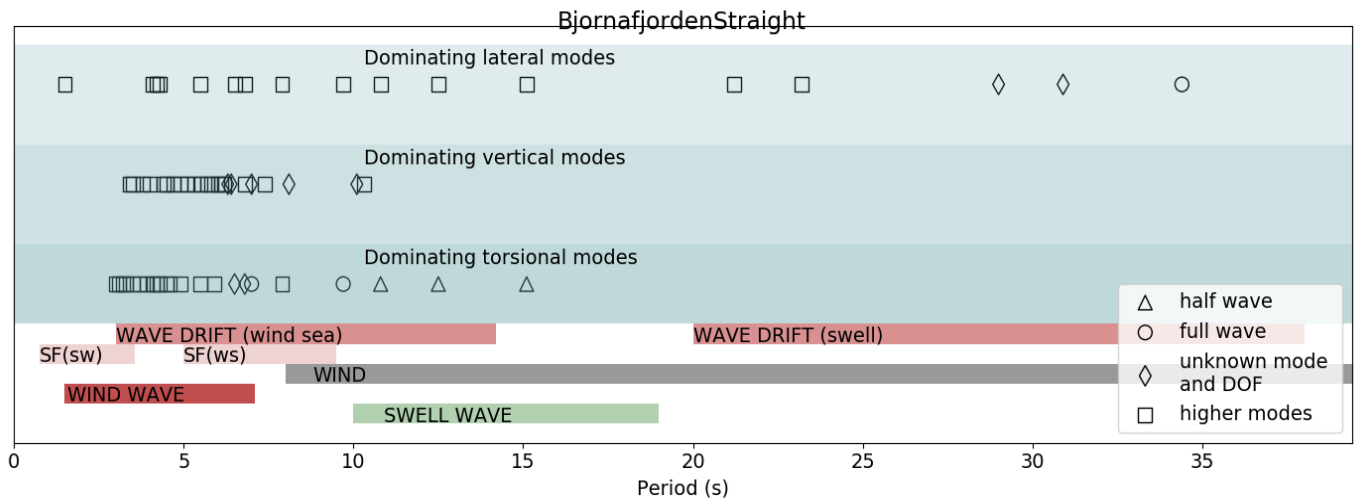


Figure 1 Observed eigenperiods and excitation load ranges for Bjørnafjorden straight bridge [5]. In addition, there is a longitudinal eigenmode at 10.3 s. See Figure 13 for layout.

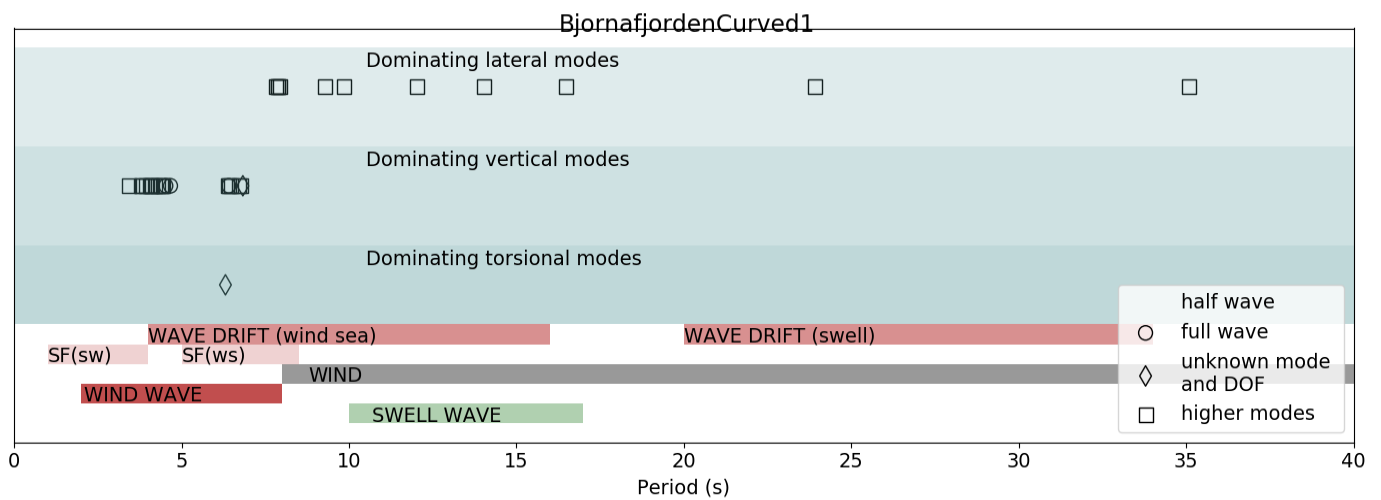


Figure 2 Observed eigenperiods and excitation load ranges for Bjørnafjorden end anchored (curved) bridge. Additional modes not included in the figure are two lateral modes of 62.55 s (1.5 wave) and 121.1 s (full wave). See Figure 14 for layout.

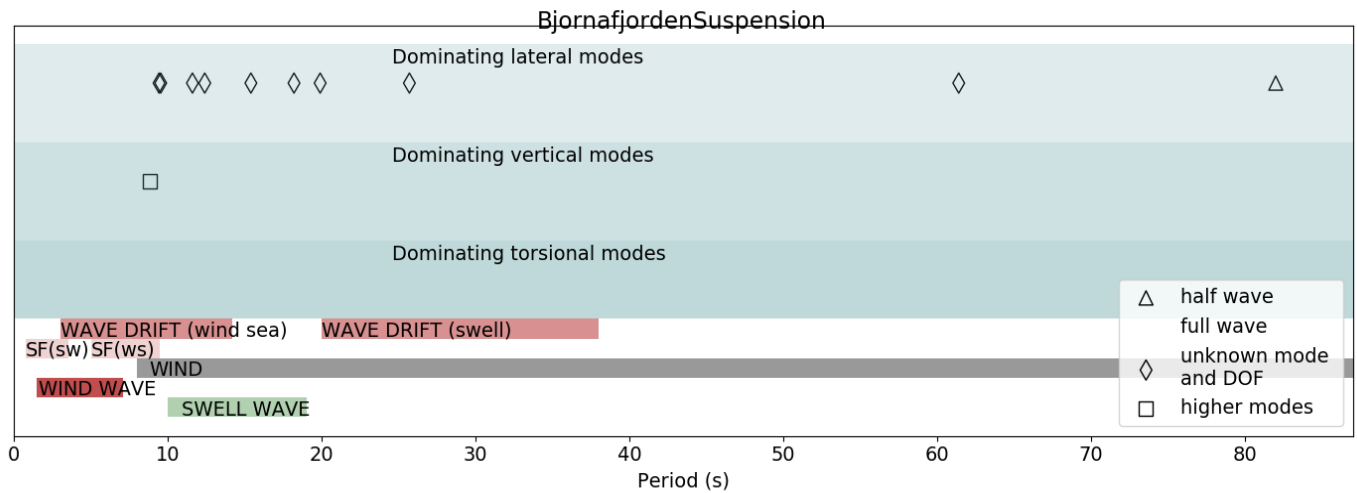


Figure 3 Observed eigenperiods and excitation load ranges for Bjørnafjorden TLP suspension bridge [7]. The main direction and mode shape were not reported for all but two modes. See Figure 15 for layout.

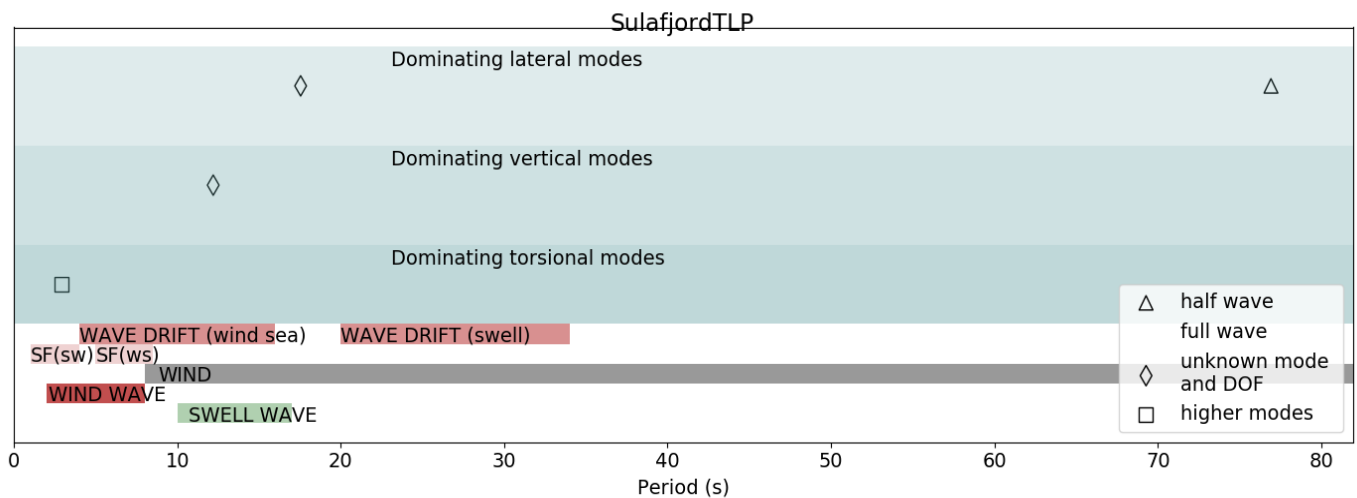


Figure 4 Observed eigenperiods and excitation load ranges for Sulafjord TLP [24] (limited number of eigenperiods reported). See Figure 16 for layout.

As an example of relative contribution from wind and waves, Table 1 shows the maximum displacements and accelerations in 1-year wind and waves for the curved Bjørnafjorden bridge. A study that compared the effects of coupling between wind and wave responses for the Sulafjorden TLP bridge [24], reported that aerodynamic loads contributed to around 80% of the lateral and vertical response.

Table 4 Motions statistics (m for displacement, deg for rotation, m/s² for acceleration) for the side-anchored straight bridge

	100 yr (static and dynamic)	Wave 1yr		Wind 1yr	
	max*	std	max*	std	max*
Vertical displacement	1.8	0.17	0.65	0.07	0.27
Rotation about bridge girder	5.7	0.45	1.7	0.12	0.42
Horizontal displacement	6.5	0.14	0.52	0.39	1.4
Vertical acceleration	1.9	0.22	0.84	0.21	0.78
Horizontal acceleration	1.5	0.14	0.52	0.03	0.1

* max denotes the 90% maximum value for a 1-hour storm condition for the 100 yr response and the expected maximum value for the 1 yr response.

Another illustrative example is taken from [11], and shows how the wind excites low frequency eigenmodes. Figure 5 and Figure 6 show the frequency content of the response, strong axis bending moment and pontoon heave motion, respectively, for a case with extreme wind and waves applied simultaneously. The sharp peaks indicate dynamic amplification of eigenmodes. One can also see the wave spectrum around 1 rad/s.

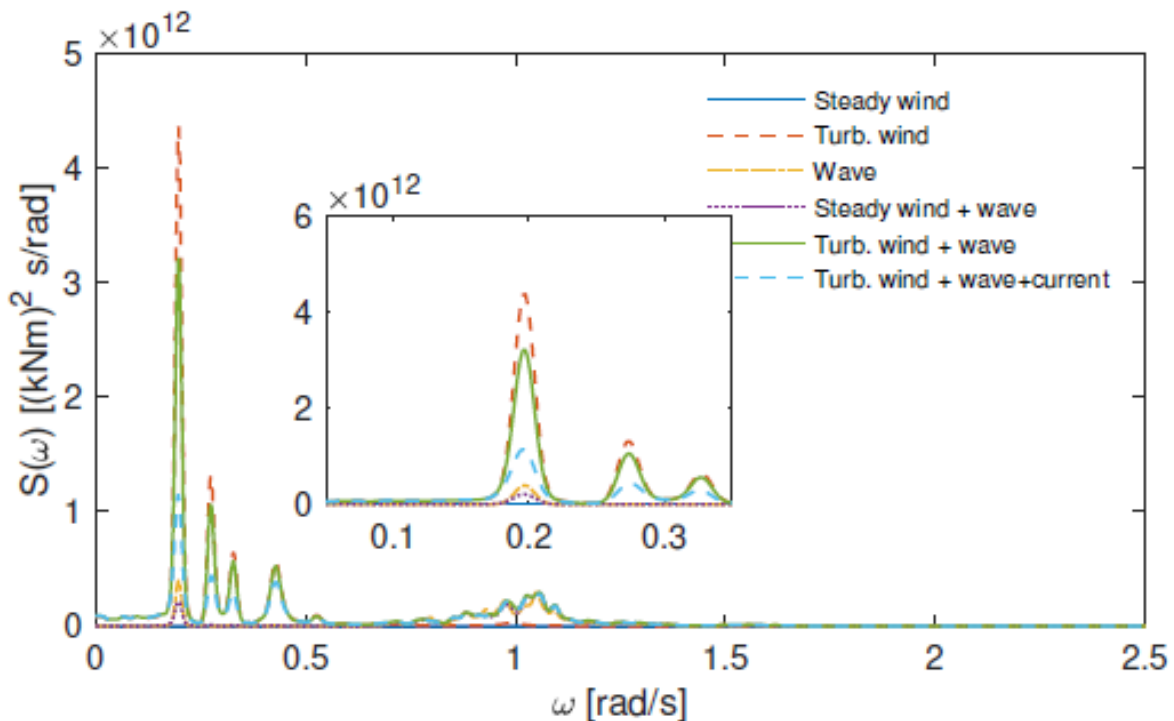


Figure 5 Variance spectrum for strong axis bending moment under extreme wind and event (from Cheng et. al. [11]). The peak around 0.277 rad/s correspond to the 3rd eigenmode.

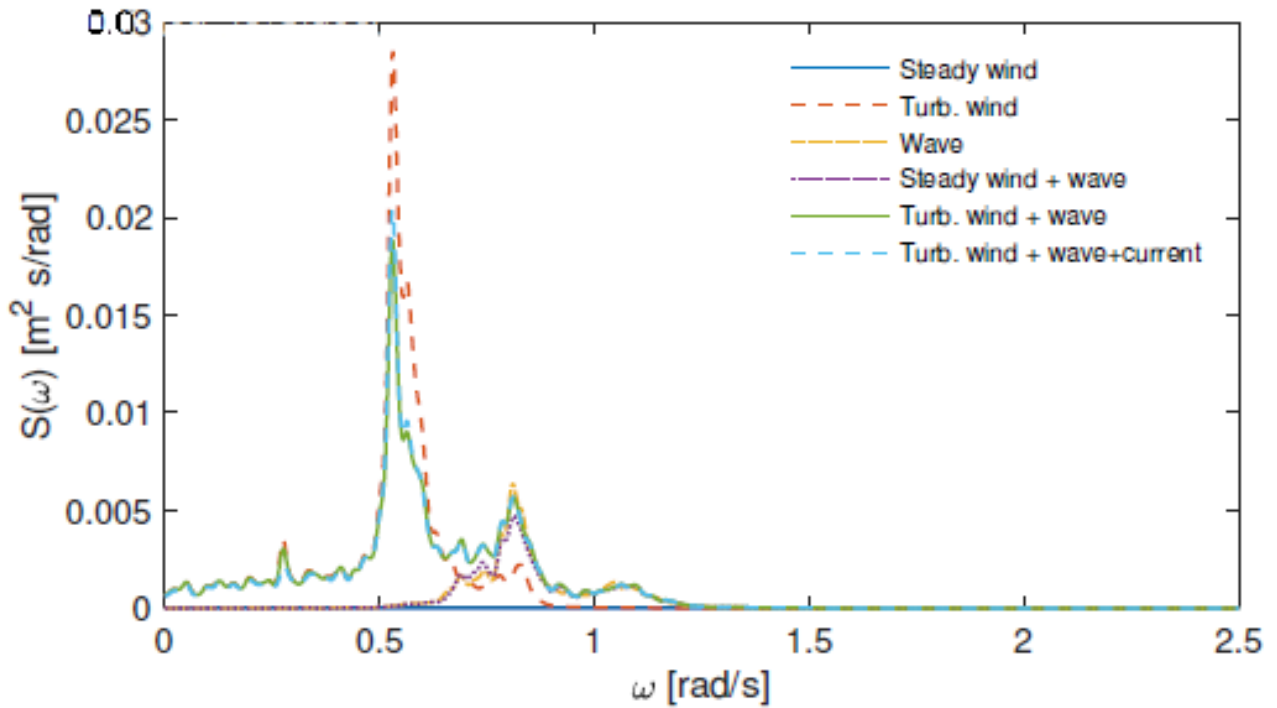


Figure 6 Variance spectrum of pontoon heave motion under extreme wind and waves (from Cheng et. al. [11]). The highest peak corresponds to vertical modes between 0.55 rad/s and 0.65 rad/s.

4.2 Global response analysis methodology

4.2.1 Hand calculations

Some responses of the bridge are simple and uncoupled and can be estimated by hand calculation. Rough estimates have been performed for more complex responses as well, as first estimates quality control of more complex analyses or screening analyses.

According to [5], the bridge girder behaves as a beam on flexible supports for vertical displacement due to static loads (traffic, self-weight). For horizontal response, it behaves as a beam which is simply supported at the north abutment (the end without the high bridge), a somewhat rotationally flexible support at the high bridge tower and fixed in the south end. The moorings act as horizontal spring supports [5].

Wind loads and static loads

As shown in a presentation by Johs Holt/Multiconsult at the LFCS workshop on 8 March 2018 [22], simple estimates of the bridge girder moment due to permanent loads and traffic have been calculated assuming beams fixed in both ends ($\frac{qL^2}{24}$ in the mid field and $\frac{qL^2}{12}$ at supports), see Figure 5. The length of these beams equals the length between pontoons.

For static wind forces in the horizontal plane, the drag force F_m on the bridge girder was calculated by:

$$F_m = \frac{1}{2} \rho V_m C_D H$$

where ρ is the density of air, V_m is the extreme mean wind velocity, C_D is the non-dimensional bridge girder drag coefficient and H is the bridge girder height. The dynamic force q_{dyn} was calculated by multiplying the static force with the turbulence intensity, what seems to be a statistic peak factor K_p of 7.0 and a dynamic amplification factor (DAF) of 1.2, assuming large damping from cables and pontoons.

$$q_{dyn} = K_p I_u F_m DAF$$

The field moment (either $\frac{qL^2}{12}$ or $\frac{qL^2}{13.8}$ depending on mooring line stiffness) was calculated assuming a beam fixed in both ends with length equal to the distance between mooring line groups.

The weak axis moment from dynamic wind loads (static vertical wind loads were considered negligible) was estimated using a function of wind velocity, turbulence intensity I_u , girder lift coefficient C_L and slope C'_L , drag coefficient and an assumed dynamic amplification factor of 2.0. This formula follows Handbook N400 [1] for wind load on bridges in wind class II, and assumes that the turbulence components can be found by multiplying the turbulence standard deviation (horizontal component $\sigma_u = V_m I_u$ and vertical component $\sigma_v = 0.55 \sigma_u$) with a statistic peak factor of 3.5 to estimate the maximum turbulence amplitude.

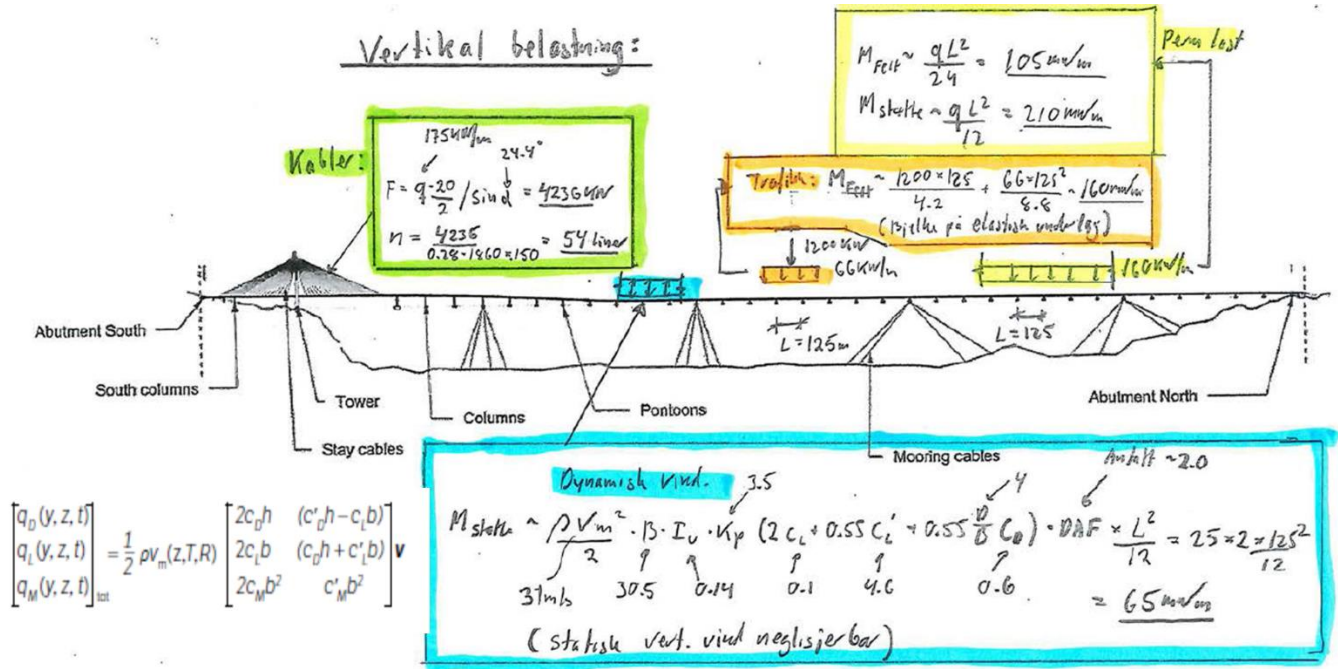


Figure 7 Hand calculations performed by Johs Holt/Multiconsult [22] together with equation 5.10 for wind load in Handbook N400 [1].

Buckling loads

The curved configuration carries part of the horizontal loads as axial forces in the bridge girder, which means that less of the load is transferred as bending moment in the bridge girder. But it also makes it unstable with respect to buckling under dynamic loading (a phenomenon also known as dynamic instability). Non-linear analysis including geometric stiffness must be used to assess the problem. For screening analyses, formulas for elastic buckling length and buckling load of curved bridge with distributed axial force were used [6].

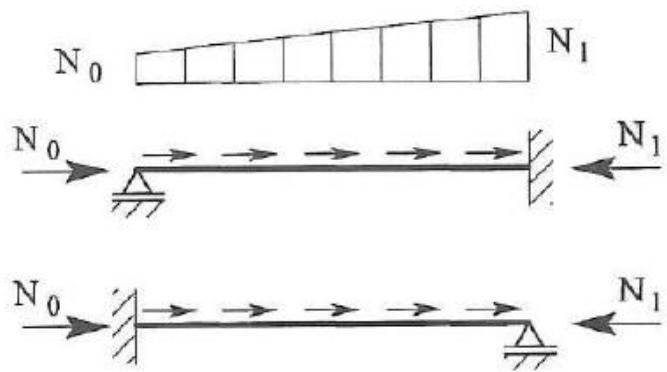


Figure 3-17 Formulas for buckling length Lk with varying axial load; axial force on the pinned end while the second formula describes L.

Figure 8 Buckling length of clamped-pinned beam-column. The first buckling mode of the curved bridge can be approximated by splitting the bridge into two sections to calculate buckling length separately. Please note that proper buckling assessment must include non-linear analysis.

Eigenperiods

Some of the eigenperiods can also be estimated using hand calculations, as described by Fredriksen et. al. [20]. They calculated the zig-zag heave mode periods (T_{nw}) from the following formula:

$$T_{nw} = 2\sqrt{(d(1 + a_{33}))\sqrt{\left(\frac{A_w}{A_w + \frac{4.8EI_y}{L^3}}\right)}}$$

where d is the draught of the pontoon, a_{33} is the heave added mass coefficient, A_w the water plane area, E the Young's modulus of the bridge girder material, I_y the bridge girder second moment of area around the weak axis and L is the distance between two pontoons.

4.2.2 Numerical methods and models

There are several numerical models established for the analysis of floating bridge response to wind and wave action. Some as a part of the conceptual design phase ([5]) and others for research studies of the importance of various modelling assumptions in wave- and wind response analysis ([10], [11], [12], [24], [26], [27]).

A general trend is the use of FEM beams for the bridge deck, tower and bar elements for cables, in solvers that have the capability of non-linear analysis (see an example in Figure 7). Multi-body-dynamic models are often used for representation of the wave forcing, but then in a coupled model with beam elements representing the rest of the structure.

All models use linear potential theory to model wave forces on pontoons and floating towers(?), and both quasi-steady and dynamic aerodynamic properties have been studied. Time-domain solvers are applied in all models, but the models are created in software packages that can also perform eigenvalue calculations, such as ABAQUS, 3DFloat and SIMO/RIFLEX. A summary of the models included in the review is given in Table 2.

Table 5 Overview of numerical models for wind and wave analysis in the review

	Structural model	Structural non-linearity	Time/frequency domain	Wave model	Wave load model	Wind model	Wind load model	Software
Bergsøysundet, Kvåle et. al. [31]	FEM beam + shell	?	Frequency	Pierson-Moscowitz, uniform with wave spreading	Linear potential theory (ignored freq. dependency)	None	No wind	Abaqus + Wadam
Bjørnafjorden, Multiconsult [4]	FEM beam+multi body	Non-linear	Time	Jonswap for wind sea with spreading, swell w/ spreading	1 st order potential theory + Newman's approximation	Turbulent (Windsim), spatial coherence, homogenous	Quasi-steady linearized coefficients, buffeting theory, aeroelastic load	Orcaflex (Sofistik for other than wind/wave loads)
Bjørnafjorden, Norconsult [5]	FEM beam	Non-linear	Time	Jonswap for wind sea and swell with wave spreading	Linear potential theory + quadratic drag	Kaimal (Turbsim), spatial coherence, homogenous	Quasi-steady coefficients, non-linear and aeroelastic load	3DFloat + Wadam (Sofistik for static analyses)
Bjørnafjorden, Aas-Jakobsen (wave analysis) [6]	FEM beam	Non-linear	Time	Jonswap + swell (spectrum unclear)	Linear potential theory	No wind	No wind	Orcaflex
Bjørnafjorden, Aas-J. (wind and static) [6]	FEM beam	Linear (incl. geom. stiffn.)	Frequency	No waves	No waves	(windsim)	Unknown (aerodyn. derivatives?)	NovaFrame
Bjørnafjorden cable stayed, Cheng [9], [11]	FEM beam + multibody	Non-linear	Time	Jonswap, homogenous and inhomogeneous	1 st order potential theory + Newman's approximation + quadratic drag	No wind	No wind	Riflex + Simo
Bjørnafjorden cable stayed, Cheng [11]	FEM beam + multibody	Non-linear	Time	Jonswap, homogenous	1 st order potential theory + Newman's approx. + quadr.drag	IEC and N400 wind spectrum	Quasi-steady coefficients, non-linear and aeroelastic load	Riflex + Simo
Bjørnafjorden TLP [12]	FEM beam + multibody	Linear	Time and frequency	Irregular (unknown)	1 st order potential theory	Turbulent (unknown)	Frequency dependent aerodyn. derivatives	Abaqus + Wadam
Sulafjord TLP, Wang[27]	FEM beam + multibody	Non-linear	Time	Jonswap, homogenous	1 st order potential theory	N400 wind spectrum	Quasi-steady linearized coefficients, state-space aeroelastic forces	Abaqus + Wadam
Lysefjord-not floating, Wang[29]	FEM beam + multibody	Linear and non-linear	Time	No waves	No waves	N400 wind spectrum	Quasi-steady non-linear and linearized	Abaqus
Bjørnafjorden DNV GL [20]	FEM beam + multibody	Non-linear	Time	Jonswap, homogenous	1 st order potential theory + Newman's approx. + quadr.drag	N400 (Turbsim) with limitations wind spectrum	Quasi-steady coefficients, non-linear and aeroelastic load	Riflex + Simo

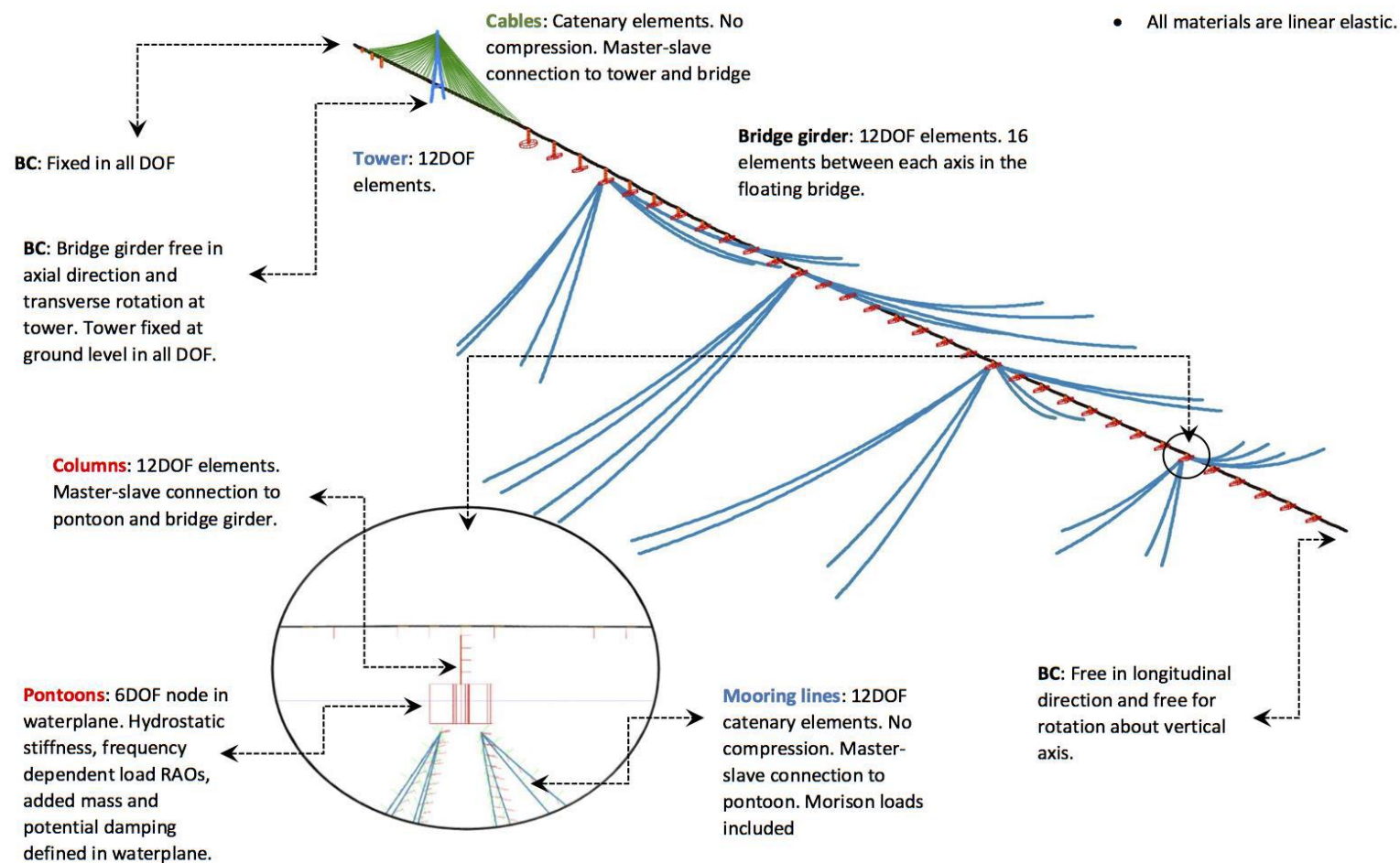


Figure 9 Example of full bridge FEM-model as modelled in Orcaflex [4]

4.2.3 Boundary conditions

Establishing the boundary conditions is important to obtain the correct responses of the bridge girder, and should be based on actual restrictions of the bridge at ends and in connection points. A boundary condition is normally given as which degrees of freedom are fixed or free. It is also possible to prescribe stiffness and damping in end- or connection points. The choice of boundary condition should either be modelled as close to real physical properties as possible, or a conservative choice should be made. It is not always straight forward to determine if a fixed or free degree of freedom provides the most conservative estimate, as it influences different responses differently.

The physical constraints for the straight bridge are described as follows in the Analysis and Design report from Multiconsult [4]:

North abutment

The north abutment consists of two concrete caissons filled with gravel, one in axis 36 and one in axis 37. The caissons are founded on shallow water, roughly 10m. At abutment north, the bridge girder will be restrained for vertical and lateral movement as well as rotation about lateral and longitudinal axes. Vertical force is taken by two bearing in axis 36 (50MN), lateral force is taken by two bearings placed in axis 37 (10 MN). In addition, 2 bearings are placed in axis 37 (35MN) to give the rotational restraint about lateral axis. The reason for placing the horizontal force bearings in axis 37 and not 36 is to reduce the lateral movement to be taken by the expansion joint. Rotational restraints are taken by force couples in the bearings and the larger the distance between bearings the smaller the forces will be. The distance between bearings is 16 m in lateral direction and 40 m in longitudinal direction. It is not allowed to prestress for uplift forces. Thus, uplift due to rotational restraints must be taken by ballast. It is decided to fill the steel box section with concrete. All bearings must have a sliding plate to accommodate for longitudinal movements of +/- 3m. At axis 37 the bridge girder can rotate about vertical axis and to move freely in longitudinal direction. To provide for the free movement an expansion joint is installed which can take movements of +/- 3 m. The movement is based on a conservative high temperature range of 91 degree according to the specification in the current Eurocode. By comparison, the former handbook HB185 (1996) assigned a maximum range of 63 degrees which is only 70 % of the current Eurocode.

Several major suppliers are conferred regarding manufacture of a joint with the considerable longitudinal movement of ca. ±3.0 m. The feedback from relevant supplier all is that they can produce a lamella/modular joint that fulfils the requirements. This is a joint type that has been in the market from various suppliers for years. According to Design Basis part 10.2/N400 part 12.5.4 the maximum gap is limited to 80 mm in SLS-Charact. With a maximum range of 5.94 m this gives $N = 5.94 / 0.08 = 74.3 \approx 75$ lamellas. This is about the double size of what has been installed earlier (around 30 lamellas) and comprises thus a component of development and innovation.

South abutment.

The abutment is a 20 m long, 30 m wide and 8 m tall concrete caisson filled with gravel. The abutment is monolithically connected to the multicell concrete box. The abutment shall take global forces coming from the bridge girder. The most significant force component is axial load in bridge girder coming from wave loading on floating bridge; in ULS 3 this axial force is approximately 80MN. Enough gravel is filled in abutment to take this force by friction towards rock ground.

In the DNV GL report [20], a summary of the boundary conditions used is given, as shown in Table 6. In addition, stay cable attachments are assumed rigidly connected to the centre of the tower, the cross-beam of the tower is connected to the geometrical centre of the tower legs and stay cable bottoms are slaved to the bridge girder.

Table 6 List of boundary conditions in DNV GL analysis [20]

Location	X motion	Y motion	Z motion	X rotation	Y rotation	Z rotation
Axis 1A	Fixed	Fixed	Fixed	Fixed	Fixed	Fixed
Bridge girder at axis 2	Free	Fixed	Fixed	Fixed	Free	Free
Axis 36	Free	Free	Fixed	Fixed	Free	Free
Axis 37	Free	Fixed	Fixed	Fixed	Fixed	Free
Bottom of column at axis 1B	Fixed	Fixed	Fixed	Fixed	Fixed	Fixed
Bottom of column at axis 1C	Fixed	Fixed	Fixed	Fixed	Fixed	Fixed
Bottom of column at axis 1D	Fixed	Fixed	Fixed	Fixed	Fixed	Fixed
Bottom of East tower leg	Fixed	Fixed	Fixed	Fixed	Fixed	Fixed
Bottom of West tower leg	Fixed	Fixed	Fixed	Fixed	Fixed	Fixed
All anchors	Fixed	Fixed	Fixed	Fixed*	Fixed*	Fixed*

* Since the anchor lines are modelled as bar elements, these boundary conditions have no effect.

4.2.4 Frequency Domain Solvers (linear)

For the screening analyses reported in [5], Orcaflex frequency domain solver was used with linearized tangential stiffness to account for non-linearities. The excitation forces here are 1st order wave forces. These are governing for the fatigue response. Second order wave force and dynamic wind forces are not included.

Here, we describe the essential components of a dynamic response analysis in the frequency domain as outlined in the theory manual of the computer program FEDAF, [35].

To derive the cross-spectral density matrix of nodal element forces from the cross-spectral density of sea elevation a sequence of operations must be performed. For each point on two arbitrary elements s and t , the product of force vectors $q_s(\omega)$ and $q_t^T(\omega)$ must be multiplied by the sea elevation cross-spectral density, $S_{\eta_s \eta_t}(\omega)$, for the sea surface projections of these points. Pre- and post-multiplication by the interpolation polynomials N_s^T and N_t is then performed, followed by a double integration to produce nodal loads rather than force intensities. Finally, pre- and post-multiplication by connectivity matrices (relating local to global dofs) are required before a double summation over all possible element pairs are carried out. The nodal load spectral density matrix can hence be expressed by

$$S_Q(\omega) = F(\omega) \cdot S_{\eta}(\omega)$$

where

$$F(\omega) = \sum_s \sum_t a_s^T \int_{l_s} \int_{l_t} N_s^T q_s(\omega) q_t^{*T}(\omega) N_t \cdot \int_{\theta} \psi(\theta) e^{-ik \cdot (x_s - x_t)} d\theta dl_s dl_t \cdot a_t$$

where,

x_s and x_t are position vectors corresponding to points on elements s and t

the matrix $F(\omega)$ is frequently termed the *hydrodynamic transfer function* of the structure-fluid system.

The double integration in this equation should strictly be carried out inside the integration over direction. This is due to the $q(\omega)$ vectors generally being dependent on the direction of wave propagation. Here, however, the hydrodynamic force is simplified to be a function only of the mean wave direction.

$$q_s(\omega) = T^T \cdot q(\omega)$$

where both vectors are six-dimensional.

By interchanging the order of integration in the above equation, the double integration over the elements can be carried out analytically. First, we introduce the notation

$$\alpha_{st}(\theta, \omega) = e^{\left\{-i \operatorname{sign}(\omega) \frac{\omega^2}{g} ((x_s - x_t) \cos \theta + (y_s - y_t) \sin \theta)\right\}}$$

where,

(x_s, y_s) and (x_t, y_t) are coordinates of node 1 of element s and t .

Furthermore, we employ

$$D_s(\theta, \omega) = \int_0^{l_s} N_s e^{\left\{-i \operatorname{sign}(\omega) \frac{\omega^2}{g} \cos \alpha \cos(\mu_m - \theta) s\right\}} ds$$

where,

μ_m is the angle between the horizontal projection of the element axis and the global X-axis

α is the angle between the same projection and the element axis itself.

Instead of the true (cubic) interpolation polynomials for the beam elements, linear functions are chosen in matrix N_s . This is not expected to affect the accuracy significantly and allows the integration above to be performed analytically without much effort.

Only a numerical integration over direction then remains, and the hydrodynamic load transfer function is expressed as

$$F(\omega) = \sum_s \sum_t a_s^T \int_{\theta} \psi(\theta) \alpha_{st}(\theta, \omega) D_s^{*T}(\theta, \omega) q_s(\omega) q_t^{*T}(\omega) D_t(\theta, \omega) d\theta a_t$$

which is more convenient for numerical evaluation.

Response spectral matrices

To derive spectral densities of response processes from those of the load components, a Fourier transformation of the equilibrium equation is first introduced. Adding the frequency dependent added mass and hydrodynamic damping matrices to the system, the relation becomes:

$$[K + i\omega C(\omega) - \omega^2 M(\omega)]r(\omega) = Q(\omega)$$

where,

matrix K also contains hydrostatic stiffness terms

$r(\omega)$, $Q(\omega)$ are the complex transformation amplitude response and load vectors, respectively.

Inserting this relation, we get

$$r(\omega) = H(\omega)Q(\omega)$$

here,

$$H(\omega) = [K + i\omega C(\omega) - \omega^2 M(\omega)]^{-1}$$

is frequently termed *the frequency response function*.

By invoking the definition of spectral density, it can be shown that

$$S_r(\omega) = H(\omega)S_Q(\omega)H^{*T}(\omega)$$

where the load matrix is expressed in terms of the hydrodynamic load transfer function matrix.

$S_r(\omega)$ is the requested response spectral density matrix of the displacement processes. Internal forces and stresses are subsequently readily derived by multiplication of element stiffness matrices

Due to the linearity of the formulation above, the Gaussian property is preserved up to the response. Expected extreme values for such processes during a specific short-term stationary condition can then be obtained. The expected number of zero crossings within a time period T is expressed as

$$N = \frac{\dot{\sigma}}{2\pi\sigma}$$

where,

σ is the standard deviation of the response

$\dot{\sigma}$ is that of the velocity process.

The expected largest maximum response during the same period is then determined as

$$E[x_{max}] = \sigma \left(\sqrt{2 \ln N} + \frac{0.5772}{\sqrt{2 \ln N}} \right)$$

The corresponding standard deviation is given by

$$\sigma[x_{max}] = \left(\frac{\pi\sigma}{2\sqrt{3\ln N}} \right)$$

There are obvious limitations associated with frequency domain response analysis for structures of the present type. This is due to the inherent assumption of linearity for such methods (unless higher-order terms are introduced). This implies that non-linearities associated with hydrodynamic loading and structural behaviour are simplified by linearization at some representative “point”. Non-gaussian response characteristics are accordingly not properly represented. Depending on how the linearization is performed, this will typically lead to over- or under-estimation of the extreme structural response level. For low and intermediate excitation levels, the assumption of linearity may still be adequate. This implies that for fatigue analysis such methods can offer an efficient and useful computational tool.

4.2.5 Time domain solvers (linear/non-linear)

Many of the numerical tools used for floating bridges have time-domain solvers that solve for equilibrium at every time step. If the equilibrium is considered for the updated position at each time step, the analysis is considered to account for geometric non-linearity.

In hydrodynamic analysis, non-linear analysis may be particularly important for moored bridges where the stiffness contribution from mooring lines depend on the displacement of the pontoons. Also, drag-type varying forces, from waves and wind, cannot be solved by linear solvers without linearization.

Considering frequency dependent hydrodynamic properties in time domain by state-space formulation is an established and validated practice in marine engineering.

Frequency- and time domain solutions gave the same response to pure wave loads, in a model robustness study reported in [8]. The frequency domain model did not include wave drift, but since the time domain model showed negligible wave drift response, it did not contribute to differences between the frequency domain model and the time domain model.

It should be noted that in case of non-linear interaction effects between wind and waves, e.g. change in stiffness from the mooring system because of wind induced displacement, these cannot be considered directly in frequency domain analyses.

4.2.6 Capabilities and performance of applied software packages

Some of the relevant computer programs for response analysis of floating bridges are already presented in Section 4.2. For analysis of static response, a wide range of different computer software can be applied. However, for analysis of dynamic response due to wind and waves the options are far more restricted. This is particularly the case for representation of stochastic wave and wind loading. The three most commonly applied computer programs for this purpose seem to be Simo/Riflex, Orcaflex and 3DFloat.

There does not seem to be any systematic comparison between results obtained by application of these programs, but still “pairwise comparisons” have been performed. In [14], dynamic responses due to irregular waves as computed by Simo/Riflex versus Orcaflex were computed for the end-anchored Bjørnafjorden bridge concept (i.e. the curved bridge). The results for the extreme responses along the bridge were overall within 10 % agreement, while the largest deviation was around 35%. It is anticipated that the discrepancies will be smaller when results for harmonic loading (i.e. regular waves) are compared, which is presently under way.

A comparison between dynamic response due to both wind and waves computed by application of the two computer programs Orcaflex and 3D Float is reported in [21]. For this more challenging case of combined load processes the discrepancies are found to be very significant (i.e. up to more than 100% for some of the responses).

What all the numerical models have in common, is that they require a large number of different cross sections with different structural-, material-, aerodynamic- and hydrodynamic properties. There are also several boundary conditions at connection points, where simplifications have to be made, in addition to a range of choices when it comes to hydro- and aerodynamic load models. Different results were obtained with different software packages (DNV GL's SIMO/RIFLEX model and Multiconsult's Orcaflex model [20]), and even within different versions of a model in the same software package. A quote from [21] illustrates some of the complexity:

Some differences [between programs] are present but the really large differences are due to different choices of input parameters that are not related to the calculation process.

As a general observation, more benchmark studies for all the programs seem to be highly relevant. Possibly this could be in the form of simplistic models to start with and then subsequently increasing the modelling complexity. This would allow to pinpoint the sources of discrepancies in a more systematic manner.

4.3 Wave loads

Floating bridges experience wave loads on all components in contact with water, i.e. pontoons, tower foundations and mooring lines. But waves also have a large influence on loads on components above the water, mainly through wave induced pontoon motions imposed on the bridge girder. For a thorough description of wave loads, it is referred to the review report for WP2. The current section focuses on the structural response to wave loads.

4.3.1 First order wave loads

For first order wave loads, all the models in this study have applied linear potential theory (see Table 2), which is generally accepted to provide accurate forces in the wave frequency range. However, one uncertainty in the use of potential flow forces is hydrodynamic interaction between pontoons. This is further discussed in 4.3.5.

4.3.2 Wave spectrum (wind sea, swell)

Wind sea contains lower wave periods than swell (see Section 4.1.3) and will excite different eigenmodes. The spreading function is also steeper for wind sea than for swell, according to the design basis [3]. At the time when the analyses included in this review were performed, a spectrum for swell that fits the

measurements were not available, and a JONSWAP spectrum was prescribed by the Design Basis, which means that there is some uncertainty in the observations made for swell response.

Wind sea measurements obtained reasonable fits for Bjørnafjorden with the JONSWAP spectrum [3].

According to the design report for the end-anchored curved bridge [5], swell triggered horizontal modes between 12-25 s, but the contribution was small compared to wind response.

4.3.3 Wave spreading

Short crested wave has been considered in many of the studies performed in the feasibility studies ([5], [6]), applying a traditional cosine wave spreading function with suitable exponents. Cheng et. al. [10] found that considering short crested waves, gave significantly higher standard deviations in vertical motion and weak axis bending moments, compared to long crested wave response. In lateral motions, the effect was less noticeable.

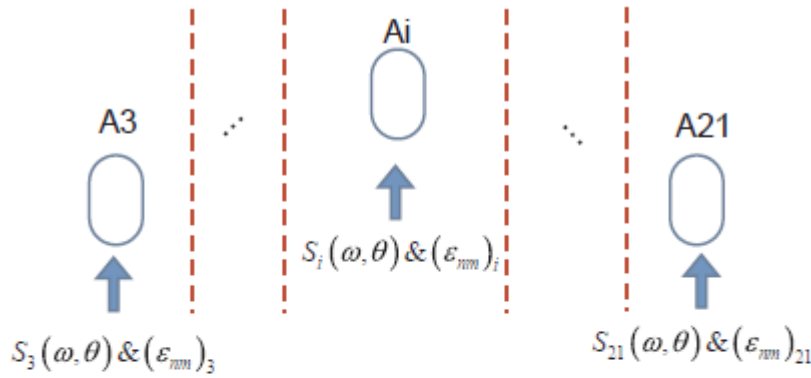
4.3.4 Inhomogeneous wave conditions across the span

Inhomogeneous wave conditions refer to varying significant wave height, peak period, other spectral parameters, direction and phase angles of harmonic components across the span of the bridge. Figure 8 illustrates the difference between homogeneous and inhomogeneous wave elevation for three pontoons. For structures far offshore, these parameters can be assumed to be constant due to little influence from seabed topology. For smaller structures in near shore areas, it may also be safe to assume homogenous waves. A long bridge crosses area with large variation in seabed topology and different levels of wave and wind disturbance from the surrounding terrain. However, inhomogeneity conditions need to be based on reliable metocean data.

In the feasibility studies in phase 3, only homogenous waves have been applied in design analyses. Cheng et. al. [11] studied the effect of inhomogeneous waves on an end anchored, curved version of the Bjørnafjord crossing. They applied pre-generated excitation forces on the pontoons as input to SIMO, with wave spectra based on interpolated parameters for each pontoon. Both first order components, slow drift and viscous drag were considered in the pre-generated force. For three different environmental conditions, three different varieties of inhomogeneity were studied and compared to the homogeneous case:

- 1) Keeping H_s , T_p and direction constant, varying the random phase angle.
- 2) Varying H_s , T_p and direction, keeping the phase angle constant for all pontoons.
- 3) Varying all parameters.

The study showed that 1) gave similar results as the homogenous case, whereas 2) and 3) gave similar results. Assuming inhomogeneous waves gave both larger and smaller standard deviations for transverse and vertical motion, axial force and strong axis bending moment in the bridge girder, depending on the environmental condition and span location.



$S_i(\omega, \theta)$: Directional wave spectra for pontoon at A_i , is a function of (H_z, T_p, θ_p)
 $(\epsilon_{nm})_i$: Random phase angle for pontoon at A_i

Homogeneous wave condition:

$$i, j \in [3, 21] \& i \neq j \quad (H_z, T_p, \theta_p, \epsilon_{nm})_i = (H_z, T_p, \theta_p, \epsilon_{nm})_j$$

Inhomogeneous wave condition:

$$i, j \in [3, 21] \& i \neq j \quad (H_z, T_p, \theta_p, \epsilon_{nm})_i \neq (H_z, T_p, \theta_p, \epsilon_{nm})_j$$

Figure 10 Homogenous and inhomogeneous wave conditions as described in [11]

The wave elevation $\zeta(x, y, t)$ is described by addition of the individual harmonic components with frequency ω_m and direction θ_m , where the amplitude is determined by the wave spectrum $S_\zeta(\omega_n, \theta_m)$. The position of the pontoon is (x, y) .

$$\zeta(x, y, t) = \Re \sum_{n=1}^N \sum_{m=1}^M \sqrt{2S_\zeta(\omega_n, \theta_m) \Delta\omega \Delta\theta} \exp[i(\omega_n t - k_n x \cos(\theta_m) - k_n y \sin(\theta_m) + \epsilon_{nm})]$$

There are currently no software packages known to the authors that provide an out-of-the-box method to apply inhomogeneous waves. The method applied by Cheng et. al. will neglect hydroelasticity, which may have an influence in the non-linear terms of the excitation. Hydrodynamic coupling between pontoons (added mass and potential damping) is neglected.

Li et. al. [15] also performed analyses with inhomogeneous waves and compared the results to a homogenous wave field. They performed analyses including hydroelasticity for one curved end-anchored and one straight side anchored floating bridge using an in-house code. The strategy in this study was to divide the span into four regions with different wave spectra and compared an extreme load condition, with H_s between 1.9 m and 2.8 m, peak periods between 5 s and 8.5 s, and wave direction normal to the bridge, to a homogeneous case where the H_s of 2.8 m was applied over the whole length of the bridge. The analysis seems to have assumed long crested sea and uniform wave direction along the length. Following this approach, the responses for both bridges were generally higher for the homogeneous waves.

4.3.5 Hydrodynamic interaction between pontoons

Depending on the distance between the pontoons of the bridge, there may be hydrodynamic interaction effects that may be important to include when performing global response analysis.

Xiang et. al. [13] performed hydrodynamic analysis and global response analysis for models with hydrodynamic interaction between the 120 m spaced pontoons and compared the results to a base case with no interaction. Examples of the resulting added mass (Figure 9) and diffraction force (Figure 10) in surge direction are shown in figures below. It was observed that piston and sloshing modes between the pontoons created spikes in the added mass and diffraction force curves, and that there are sheltering effects from upstream pontoons on the diffraction force. The same was also seen in when performing similar analyses in the model robustness study performed for the Bjørnafjorden straight bridge [8].

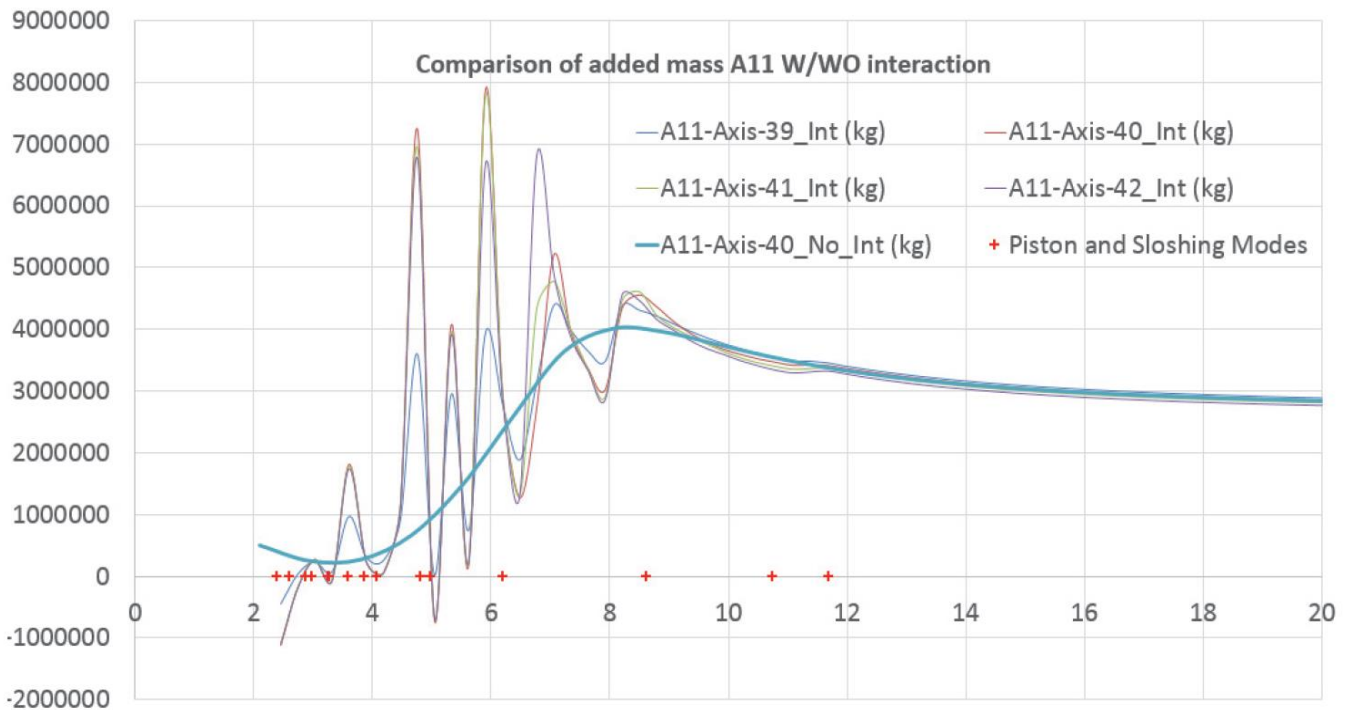


Figure 11 Added mass in surge direction for four interacting pontoons compared to a pontoon with no interaction [13]

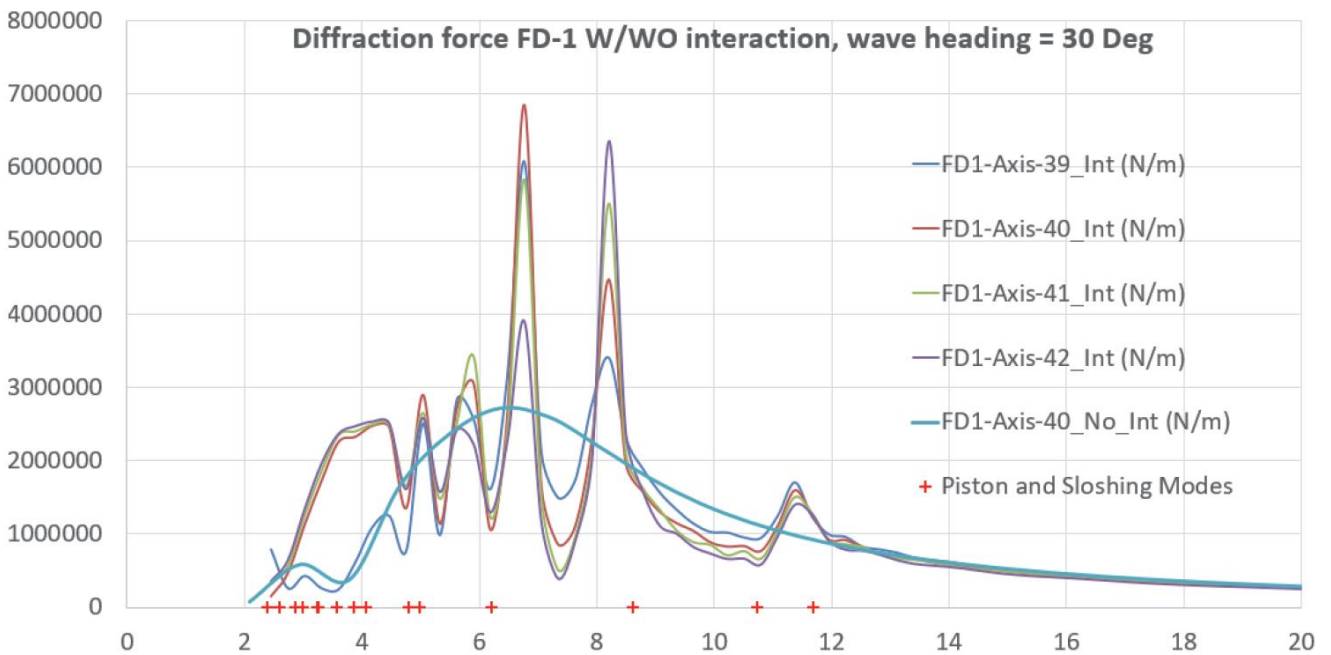


Figure 12 Surge diffraction force transfer function for four interacting pontoons compared to a pontoon with no interaction [13]

Xiang et. al. also compared the implications of hydrodynamic interaction on global response, for a few demonstration cases (bridge deck moments, motions and accelerations at the intersections with the pontoons). For waves propagating along the bridge, there was a notable sheltering effect, that reduced the weak axis bending moments. For waves perpendicular to the bridge, diffracted waves between the pontoons led to increased weak axis bending moments compared to the case with no hydrodynamic interaction.

The hydrodynamic interaction effects are of course dependent on the pontoon spacing. But the main conclusion seems to be that for pontoon spacing around 100 m, they should be carefully considered. It has also been highlighted that there is some uncertainty in the effect of viscous damping, which is not considered in potential flow solvers. There are various methods to handle this, e.g. through tuning of viscous drag coefficients to model tests.

However important the interaction effects may be, it is not straight forward to include them properly in global response analysis. Firstly, it is computationally expensive to solve the radiation/diffraction problem using boundary element computation tools. Secondly, global analysis software using coupling between structural model and the hydrodynamic body model do not always account for the full interaction, only the body specific parts (diagonal matrices).

4.3.6 Second order wave loads

Second order wave loads consist of so-called sum and difference frequency excitation forces. These forces contain less energy than first order wave forces but can excite motions at frequencies above or below the wave frequency range. Long, floating bridges will typically have long natural periods, and difference-frequency loads, also often referred to as slowly varying- or drift forces, can be important. However, they do

often excite the same eigenmodes as the wind, and the slowly varying wave induced motion may be negligible in comparison.

Slow drift forces were included in the analyses performed for the Bjørnafjorden crossing for both the straight moored bridge [5] and the end-anchored bridge [10] and [11], through applying Newman's approximation. The validity of Newman's approximation in short crested waves is, however, questionable [5].

Sum-frequency forces are from oil&gas platforms known to be important for heave on tension-leg platforms, due to the low eigenperiod of heave motion. For the concept with TLP-pylons [7], sum-frequency forces were addressed by a sensitivity analysis but excluded from the full analysis. Compared to platforms in the offshore industry, wave periods are much shorter for coastal bridges, and thus the frequency range where sum-frequency forces occur, is much smaller. This can also be seen on the sum-frequency bar in e.g. Figure 2.

Second order wave forces on a body depend on the velocities of the body itself, and thus wind induced motions will influence the second order wave forces. The second order wave forces on a pontoon will also be influenced by the response of the entire bridge, thus iteration between potential flow solver and global model should be made when determining the forces. This has not been performed in the feasibility studies.

4.3.7 Waves from Passing Vessels

The speed with which a vessel can pass under the bridge is restricted, but an accidental limit state has to include a rough wave from vessel passing with some higher speed than the speed limit. The Design Basis [16] prescribes three vessel induced waves for ships passing at different speeds.

4.4 Wind Loads

The long floating bridges that are the topic of this study will fall under Wind Load Class III (Vindlastklasse III), as defined by Statens Vegvesen's handbook in bridge design [1] since the span length is longer than 300 m and the highest eigenperiod is larger than 2 s. This section on wind loads will therefore refer to requirements for Wind Load Class III.

4.4.1 Aerodynamic Loads

Wind loads on a bridge girder, tower and cables consist of:

- Steady components
- Aeroelastic (motion-dependent) components
- Buffeting (motion-independent) components
- Vortex shedding
- Motion induced instabilities (static divergence, flutter, galloping)

Aerodynamic force coefficients have been included in wind load models in various ways:

- Quasi-steady with coefficients dependent on angle of attack
- Quasi-steady, assuming linear approximation of the steady aerodynamic coefficient curve
- Frequency-dependent coefficients (aerodynamic derivatives – can be used to represent vortex shedding)

Note that the term 'buffeting theory' is often used about both buffeting and motion-dependent components [2].

A wind tunnel section model test of two different bridge deck sections was carried out [16], and reported the static wind coefficients and slope with respect to angle of attack. A report from Multiconsult/Rambøll [17] estimated coefficients for two other bridge cross sections based on known values for geometrically similar sections, and also by CFD.

Further description of aerodynamic load methods is covered by the review in WP2, but the load effects will be covered by this report. Aeroelastic loads and aerodynamic instabilities are caused by the response of the structure. Since there are close connections between load and load effect, some topics related to loads will also be discussed here.

The second order velocity terms in the buffeting forces can be either included in full or linearized. Wang et. al. [26] compared wind buffeting response for the Lysefjord bridge (446 m span) a non-linear and a linearized buffeting theory model and found only small deviations in the response.

Xu et. al [12] developed a state-space formulation to include frequency dependent aerodynamic derivatives in time-domain simulations of aerodynamic loads. The model was compared to a frequency domain model with good results.

4.4.2 Vortex Induced Vibrations (VIV) and Aerodynamic Instabilities

Vortex induced vibrations

Vibrations cause by vortex shedding in wind or current flow need to be considered in the design of the bridge. These vibrations are self-limiting, but occur at low wind speeds, and need to be considered in fatigue calculations. For VIV induced by wind, design rules are given in [1]. Structural damping to be used for the fatigue calculation depend on bridge type and can be found in [1], but these values may not be valid for long floating bridges.

On a bridge girder, physical VIV suppression can be installed, e.g. by spoilers. For a suspension or cable stayed bridge, cables are known to be particularly sensitive to VIV.

A sensitivity study for VIV was performed by Aas-Jakobsen [6], who concluded that the response due to vortex shedding was small for both the bridge girder and the cables. However, they emphasize that this can increase if mass or damping is reduced.

Static divergence

Static divergence is cause by negative contributions to the structure torsional stiffness from motion induced torsional aerodynamic forces. The critical wind speed criterion is given in [1].

Flutter

Flutter in the bridge girder is caused by negative damping and typically occurs at high wind speeds with coupling between torsion and vertical translation [2]. The handbook criterion is, as for the other instability phenomena, a definition of critical wind speed for flutter onset.

Since flutter occurs for a coupling between torsion and vertical translation, the floater induced motions will influence the occurrence of the phenomenon. Multiconsult aerodynamics report for straight floating bridge reports some studies performed for various pontoon shapes and materials [17], and concluded that the 125 m spaced steel diamond shape is robust in terms of aerodynamic stability, but that further analysis needs to be performed, e.g. multi-modal analysis, which is also reported in [17]. Also, examination of flutter due to girder motions remains.

In the multimodal analysis, it was found that the conditions for flutter occurring were present, but that the significant hydrodynamic damping could limit the excitation. The multimodal analysis was performed in line with industry practice, which is to disregard transverse motion of the girder. The report points out the possible weakness of this assumption in the case of long floating bridges, because transverse motion and torsion are coupled. They also recommend performing the study with aerodynamic derivatives from wind tunnel tests.

Further limitations of the multimodal flutter analysis were that the hydrodynamic damping was determined in a different analysis tool than the aeroelastic model. And there were discrepancies between the modes in these FEM models. This is an uncertainty when it comes to estimating the correct hydrodynamic damping for the aeroelastic analysis.

Galloping

Galloping is an instability phenomenon caused by forces normal to the main wind direction. The bridge design handbook [1] uses a critical wind speed criterion, and it needs to be documented that the wind speed is below the critical wind speed. The critical wind speed is a function of bridge cross section and lowest natural frequency of the structure. Galloping occurs if the lift coefficient slope ($C_L(\alpha)$ -slope) is negative, but a small positive slope could mean that the section is sensitive to galloping [16].

The wind tunnel section model tested $C_L(\alpha)$ -slope for two different cross sections in [16], by testing with and without traffic box. The tests showed potential galloping sensitive behaviour of the tested cross sections.

4.4.3 Effect of Wind Spectrum

Since the eigenfrequencies of the long bridges are low, it is important to represent the low frequency variations in wind speed. This means that 10-minute simulation time is most likely insufficient to catch extreme responses caused by wind excitation. It also means that the amount of energy in low frequencies in the wind spectra applied in load analysis will influence the response.

Cheng et. al. [11] compared response to the IEC Kaimal wind spectrum to analyses with the N400 wind spectrum, which has more low frequency content than the IEC Kaimal spectrum (see Figure 13). They found that the mean values of the responses were quite similar between the two spectral models, but the N400 spectrum gave larger standard deviation than the IEC spectrum, which was attributed to dynamic amplification of the 3rd horizontal eigenmode (22.7 s) of the curved bridge. The difference was largest in the bridge girder axial force, the N400 spectrum gave more than 30% larger standard deviation than the IEC spectrum. Overall, the N400 spectrum gave larger standard deviations for all the considered responses (axial force, strong- and weak axis moments, torsion, horizontal and vertical motion of the pontoons).

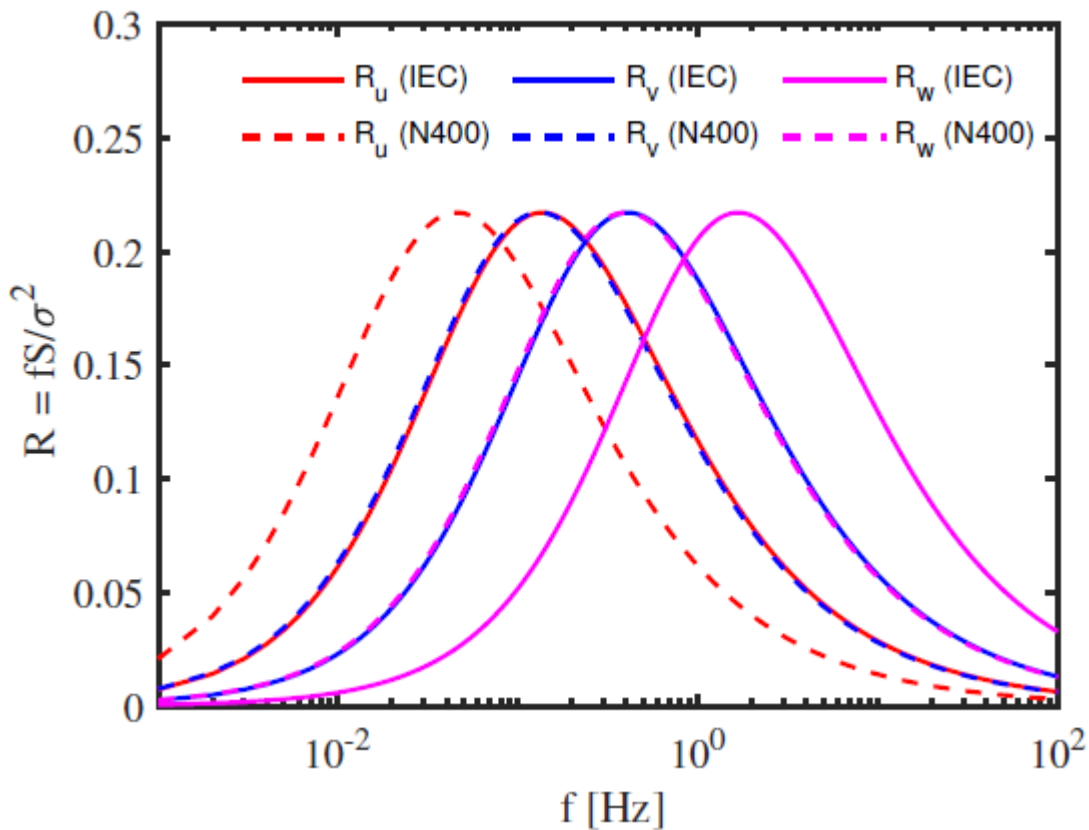


Figure 13 Normalized turbulence spectra in wind direction (subscript u), lateral direction (v) and vertical direction (w) for the IEC Kaimal and the N400 Kaimal spectra, as shown in [11]

However, these were for analyses with wind only. The importance of the spectrum for the horizontal response and axial force in the bridge is as expected, since the wind forces are known to have a large contribution to horizontal motion. Wave forces are, however, expected to have the most significant contribution to vertical motions. The analyses in [11] showed that wind forces contributed to 40-50% of the vertical motions of the pontoons in an extreme condition. In the wind spectrum comparison, the N400 spectrum gave around 20% higher vertical pontoon motion than the IEC spectrum, which was explained by dynamic amplification of vertical modes around 11 seconds. This leads to around 10% difference between the spectra when considered together with waves.

The possible sensitivity to wind spectrum low frequency content was also highlighted by DNV GL [20].

Also, in a study by Salvatori and Spinelli ([35]) of turbulence coherence across the span on a thousand-metre-long suspension bridge, concluded with the following:

Considering fully correlated turbulence can result in an important underestimation of the structural response, especially if the structure is dominated by antisymmetric modes, as can happen for suspension bridges. Therefore, along-span coherence should be considered in the bridge design.

A study on sensitivity to length scale factor was also performed by Multiconsult [7], who found up to 25.8% difference in bending moments.

4.4.4 Inhomogeneous Wind Field Across the Span

Inhomogeneous mean wind speed conditions across the planned route for the Sulafjorden bridge has been documented, see e.g. Wang 2018 [25] (only shown in presentation, not in paper). However, the work on documenting the wind conditions is in an early stage, and suitable turbulence spectra are yet to be found. (ref WP1).

Wind conditions can be inhomogeneous in mean wind speed, wind direction, turbulence and wind shear. No studies covering the effect of inhomogeneous wind conditions across the a very long span on the response have been found in this review. Chenyet et. al. [30] analysed measurements at several points on the Lysefjord bridge, and could not completely confirm homogeneous wind conditions in all wind directions. They conclude as follows:

For ultra-long span suspension bridges in mountainous environments, the lack of flow uniformity along the span may call for a modified design approach.

4.4.5 Effect of Wave on Vertical Turbulence

In the wind model test [16], a free-surface boundary test was carried out in the wind tunnel, to estimate the influence of waves on the vertical turbulence component, and its effect on the bridge vertical response. Two different waves were run, measured at three different elevation above the mean sea level, and for 5 different eigenfrequencies for the bridge.



Figure 14 Model set-up for the wave influence experiment with a travelling wave floor in the wind tunnel. In the middle of the photograph, the bridge section model (1:40) can be seen [16].

It was found that the wind velocity standard deviation in the vertical direction could increase with a factor of up to 5.5 (for 30 m/s wind and 5.32 m wave), and the turbulence increased with increasing velocity. It was also found that the wave induced vertical turbulence was very narrow banded with a clear peak at the wave frequency. This was shown to increase the response at eigenfrequencies around the wave frequency, but no significant difference from the ambient turbulence excitation was seen for eigenfrequencies away from the wave frequency.

The model test report proposes a basic relation between wave height(H) and length (λ) and wave induced wind standard deviation (parameters are explained in [16]).

$$\sigma_{\text{wave}} = k_1 \frac{H}{\lambda} (U - c) \exp\left(-k_2 \frac{z}{H}\right).$$

The report also proposes an expression for the standard deviation of the vertical bridge deck response to wave induced wind turbulence (parameters are explained in [16]):

$$\sigma_{z,\text{wave}} = \frac{1}{\sqrt{2}} \frac{\frac{1}{2} \rho U \left(b \frac{dC_L}{d\alpha} + hC_D \right) l \pi}{k} \frac{\pi}{\delta} A_w |J(U_r)|.$$

Only vertical excitation was studied in [16], and it was recommended to continue studying the effect on aerodynamic moments and rotational responses of the bridge deck.

The wave height and the distance between the mean water level and the bridge girder is important when evaluating the effect of waves on the wind turbulence, and whether or not it impacts the response of the bridge girder. The 100-year wave has an H_s of 2.4 m in Bjørnafjorden, which means a maximum wave of about 4.8 m. The bridge girder in the low part is around 15 m above the mean water level for both the straight and the curved bridge. This topic needs further consideration.

4.5 Current Loads

In addition to the static contribution to viscous forces from currents, vortex shedding can occur and cause dynamic loads that contribute to fatigue. According to the design basis, vortex induced vibrations shall be considered in mooring line loads. This is not specified but could be related to VIV on the mooring lines only or VIV of the pontoons only. The topic has not yet been addressed in the feasibility studies.

4.6 Other Loads

Fatigue from tidal variations and traffic loads are to be calculated using a combination formula given in the design basis [16]. The approach assumes that a long-term stress range distribution has been established for the response to environmental loads. The methodology was established by DNV GL in 2018 and does not seem to have been published yet.

$$D_{yrl} = f_t \sum_{i=15} p_i \sum_{j=1k} 1 \text{an}_j (\Delta\sigma_{wj} + \Delta\sigma_i + \Delta\sigma_{\text{tide}})_m + \sum_{i=15} (f_i - f_t * p_i) \sum_{j=1k} 1 \text{an}_j (\Delta\sigma_{wj} + \Delta\sigma_i)_m + (1 - \sum_{i=15} f_i \sum_{j=1k} 1 \text{an}_{mj} (\Delta\sigma_{wj} + \Delta\sigma_i))$$

where f_t is the fraction of tidal cycles relative to the number of environmental cycles, p_i is the fraction of lorry type i relative to the total number of different lorry types, f_i is the fraction of lorries of type i relative to number of environmental cycles, n_j annual number of cycles in stress block j , a is the intercept of the S-N curve with the logN-axis, m is the negative inverse slope of the S-N curve, $\Delta\sigma_{wj}$ is the stress range at hot spot due to environmental action in in block j and $\Delta\sigma_i$ is the stress range at hotspot due to lorry type i .

4.6.1 Permanent loads

Permanent load for the bridges is the self-weight of the main structure in addition to asphalt, railings and other non-load-carrying, but permanently installed part of the structure. The load effect is calculated in static analysis and is also included as mass and gravity in the dynamic analyses.

Applying design by partial factors, different load factors are applied to permanent loads and environmental loads. Since gravity is normally also included in dynamic analysis, the response to permanent loads must be subtracted from the maximum observed response under dynamic, environmental action.

4.6.2 Water level variations

Due to tides, the pontoons on the straight bridge are estimated to move up and down up to 0.73 m (depends on pontoon heave stiffness), and additional variation in vertical position is expected due to storm surges (+0.64/-0.5 m for a 100 year condition) [4]. Tidal loads are handled in static linear analysis in Sofistik for the straight bridge [4]. Fatigue due to tidal loads are calculated using stress ranges based on envelope values of the weak axis bending moment in the bridge girder.

The fatigue contribution from tide is to be calculated based on a long-term distribution of tide, and then calculate the total contribution as an equivalent stress range according to the following formula [16]:

$$\Delta\sigma_{tide} = \left(\frac{\sum_{j=1}^k (\Delta\sigma_{tide j})^m n_j}{\sum_{j=1}^k n_j} \right)^{\frac{1}{m}}$$

where k is the number of stress blocks, $\Delta\sigma_{tide j}$ is the stress range in block j due to tidal variation, n_j is the annual number of cycles in stress block j and m is the negative inverse slope of S-N curve, set to 3.0, as it is assumed that the stress range due to tidal variation should be combined with the left part of the S-N curve.

Storm surge is included in the analysis of extreme environmental conditions and will thus be accounted for in the ultimate limit state.

4.6.3 Temperature loads

Temperature loads are handled in static linear analysis in Sofistik for the straight bridge [4]. Expansion due to temperature depends on the length of the bridge, and in the case of a very long bridge, the expected temperature expansion range is large. For the straight bridge, longitudinal movement of ± 3.0 m is expected. This creates challenges for the expansion joints at the abutments.

4.6.4 Traffic loads

Traffic loads are considered in linear static analysis. In addition, they must be included when calculating fatigue. The amplitudes of the stresses from traffic were calculated based on the weight of the expected vehicles types and the number of cycles was based on a table with expected number of vehicles within each vehicle group, as shown in Figure 15:

Table 17-3 Load model FLM4

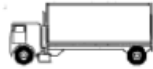




VEHICLE TYPE			TRAFFIC TYPE			
1	2	3	4	5	6	7
			Long distance Lorry percentage	Medium distance Lorry percentage	Local traffic Lorry percentage	Wheel type
	4,5	70 130	20,0	40,0	80,0	A B
	4,20 1,30	70 120 120	5,0	10,0	5,0	A B B
	3,20 5,20 1,30 1,30	70 150 90 90	50,0	30,0	5,0	A B C C
	3,40 6,00 1,80	70 140 90 90	15,0	15,0	5,0	A B B B
	4,80 3,60 4,40 1,30	70 130 90 80 80	10,0	5,0	5,0	A B C C C

Table 17-4 Number of stress cycles from traffic per year

Traffic type	Lorry 1	Lorry 2	Lorry 3	Lorry 4	Lorry 5	Total
Long distance	175 200	43 800	438 000	131 400	87 600	876 000
Medium distance	350 400	87 600	262 800	131 400	43 800	876 000
Local traffic	700 800	43 800	43 800	43800	43 800	876 000

Figure 15 Vehicle types and number of stress cycles from each vehicle type, taken from [4].

It is assumed that the bridge is closed for traffic when wind speeds are stronger than the 1-year wind. For this reason, no traffic loads are combined with wind and wave loads in 100 year and 10 000-year conditions. The maximum vertical displacement during traffic loading is 1.8 m.

4.7 Effects of interaction between loads

A quotation from the Robustness and sensitivity analysis report (Statens vegvesen / Multiconsult) [7]:

Hydrodynamic forces may initiate movement that trigger aerodynamic effects. On the other hand, aerodynamic damping might reduce dynamic effects of the hydrodynamic response. Thus, the system is complex, and it is not necessarily straight forward to evaluate the system.

Wind-wave-interaction in responses may be an important factor when designing floating bridges. Interactions with current induced response can also have an effect. Interaction effects expected to be of some importance in are:

- 1) Aerodynamic damping on wave-induced resonant motions.
- 2) Hydrodynamic (wave) damping of wind-induced resonant motions.
- 3) Effect on wave drift forces and viscous forces from wind-induced velocity of the pontoons.
- 4) Damping due to current on wind- and wave induced motions.
- 5) For a bridge with non-linear mooring stiffness, the static offset caused by the mean wind force may give different mooring stiffness compared to the non-deformed configuration, which could give different response to wave loads than if wave load were considered separately.
- 6) If lateral displacement caused by wind and/or current is large compared to the length of the bridge, geometric stiffness may influence the response to waves.

Ideally, wind, wave and current should be included in the same analysis to make sure that complex, and maybe unexpected effects will be modelled. However, this is often difficult in practice, due to limitations in the existing software packages. Existing software for hydro-elastic analysis do not contain sophisticated aeroelastic models found in traditional software for bridge design, and vice versa. Also, hydro-elastic response analyses are normally performed in time-domain, whereas frequency domain analysis has been standard practice for wind response analyses within bridge engineering.

Some effort on investigating the importance of coupled wind- and wave analysis have been performed, e.g. by Wang et. al. [24], who found that superposition of wind- and wave response ("Aero+Hydro" in Figure 16) gave good correspondence with the fully coupled response.

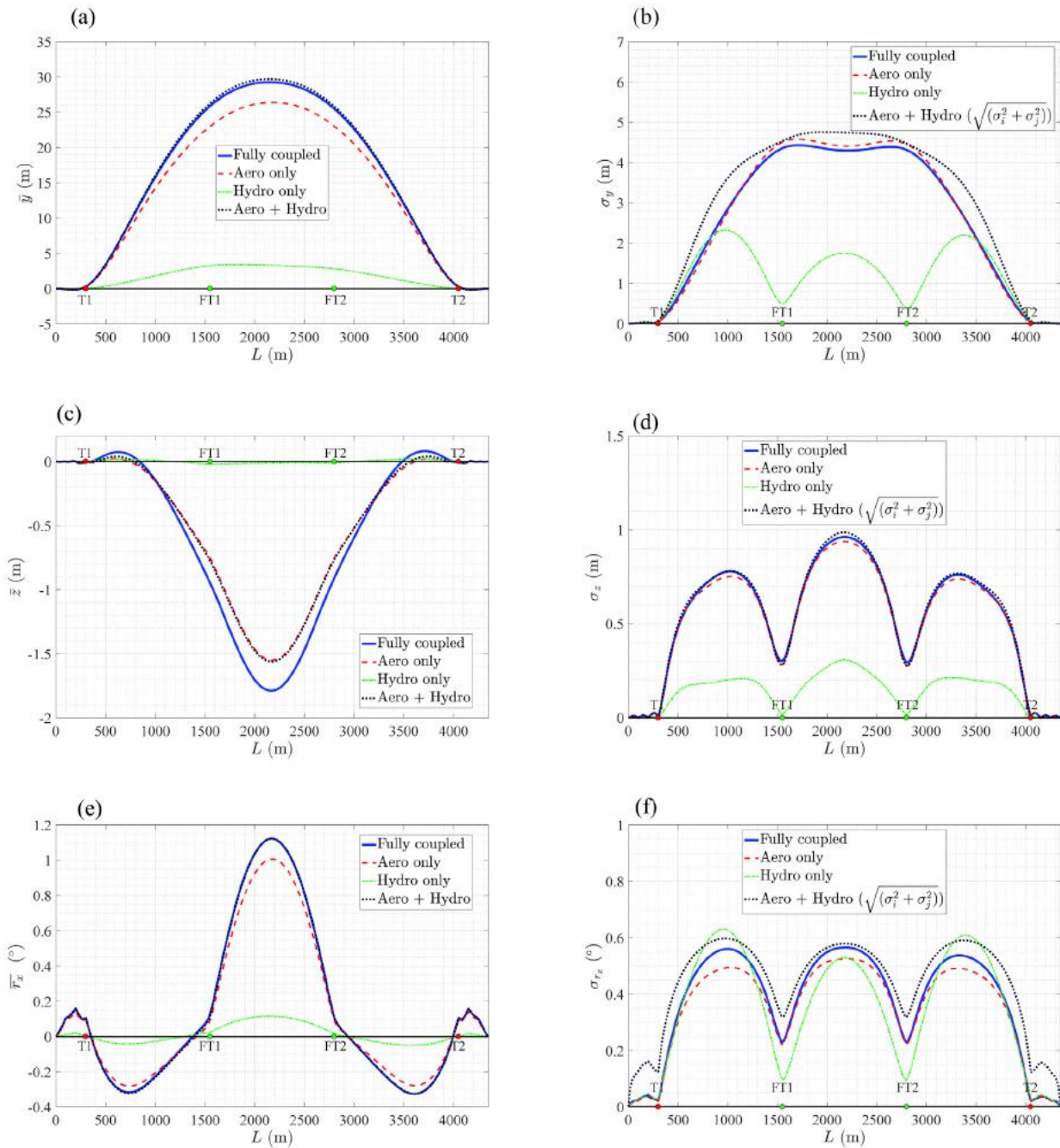


Figure 16 Effects of full coupling of wind and wave induced span deflections for the Sulafjord TLP bridge [24], lateral (a,b), vertical (c, d) and torsional (e, f).

Aerodynamic flutter induced by wave motion can also be considered an interaction effect. This is described in Section 4.4.2.

4.8 Mooring design

4.8.1 Description of straight bridge of Bjørnafjorden

4 of the pontoons are anchored by 8 anchor lines each, as shown in the Figure 17 and Figure 18. The system can be characterized as taut to semi-taut with bottom chain, wire and top chain. The purpose of the anchor lines is to restrict the transverse, horizontal offset and thereby restrict the transverse horizontal support forces at the bridge ends, as well as the curvature about the vertical (stiff) axis.

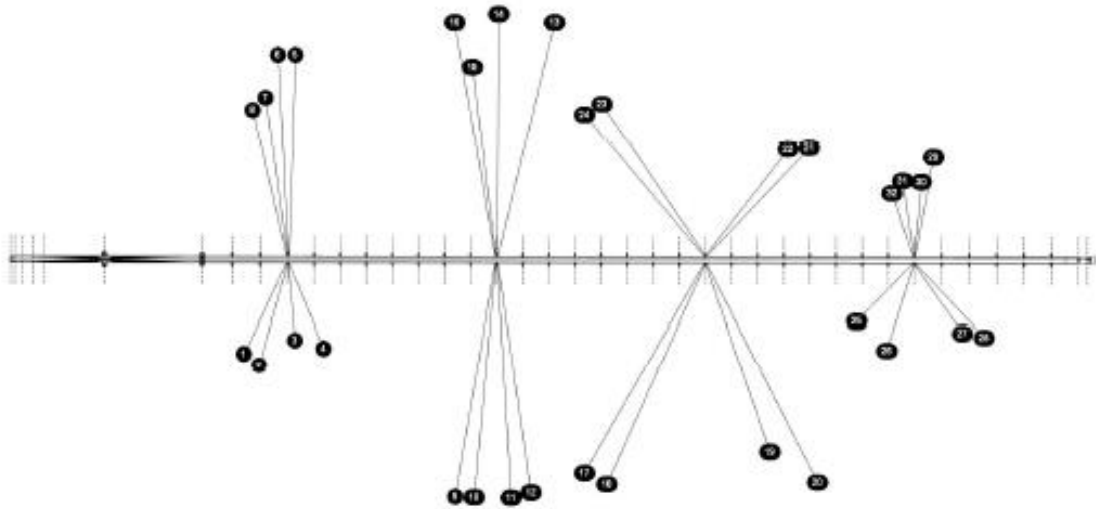


Figure 4-1 Mooring system layout including line numbering

Figure 17 Mooring system layout, top view, taken from [22].

The difference in line patterns reflects depth variation along the bridge as well as different soil conditions, with regard to anchor holding conditions.

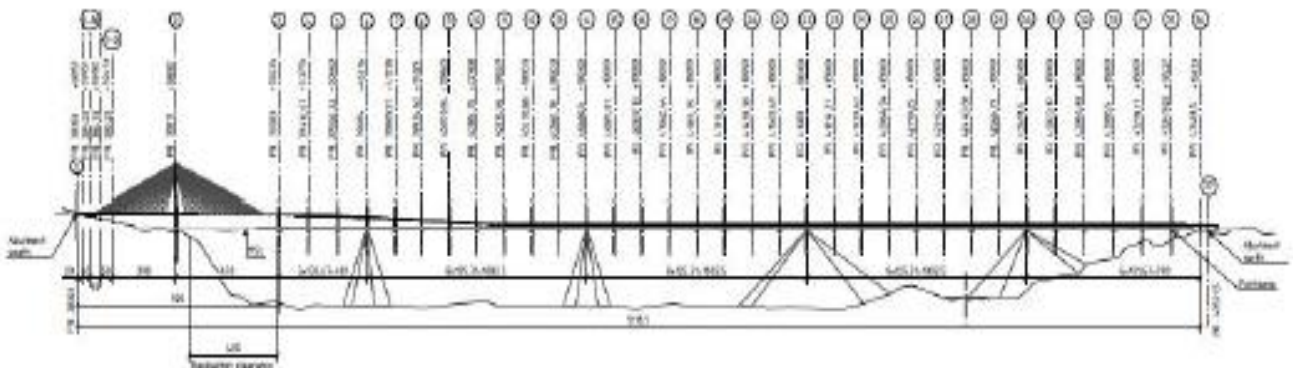


Figure 1-1 Straight floating bridge, base case 125 m with steel pontoons

Figure 18 Mooring system layout, side view, taken from [22].

The basic features of the selected anchor system are:

1. *Spacing* between anchored pontoons is about 1000 m (each 8. pontoon with 125 m spacing).
2. *Target stiffness* in the transverse horizontal direction is 1.5 MN/m for each anchored pontoon. This is obtained by adding contributions from 4 lines to each side of the bridge.

Technical challenges related to soil conditions and anchor types and anchor location have not been part of this review.

4.8.2 Uncertainties

The functional considerations of the mooring system, ensuring the structural integrity of the bridge beam, are not explicitly mentioned in the Design basis for Mooring and anchor design [17]. They are however, summarized in the DNV GL report [20], with reference to functional requirements to consequence class 3 in annex B2 of ISO 19990-7. The criteria listed here refer to safety factors and motion limitations.

Table 7 Mooring system safety factors, taken from [20].

Table 3-29 Required safety factors

Condition	Environmental condition			Traffic load	Damage	Safety factor
	Wind	Wave	Current			
ULS	100 years	100 years	100 years	No	Intact	2.20
ALS	100 years	100 years	100 years	No	One line	1.50
ALS	100 years	100 years	100 years	No	Two lines	1.35

Table 8 Motion limitations, taken from [20].

Table 3-30 Motion limitations

Motion limitation	Load case	Maximum motion	Unit
Vertical deformation from traffic loads	0.7x traffic load 1)	1.5	m
Rotation about bridge axis from traffic loads	0.7x traffic load 1)	1	deg
Rotation about bridge axis from environmental loads (RMS value)	1 year storm	1	deg
Rotation about bridge axis from static wind load	1 year static wind	0.5	deg
Vertical acceleration (RMS value)	1 year storm	0.5	m/s ²
Horizontal acceleration (RMS value)	1 year storm	0.5	m/s ²

1): Design characteristic loads

Factors influencing requirements to mooring line stiffness and spacing

- The *maximum spacing* of moored pontoons, and corresponding *minimum capacity* of the mooring, is governed by the horizontal transverse load intensity and the resistance moment of the bridge beam about the vertical axis.
- The *minimum stiffness* of each pontoon mooring is more difficult to determine. This is governed by the allowable half-wave deflection of the bridge beam from the straight line, which means higher stiffness for fewer moorings, lower stiffness for more moorings.
- It could be useful, in future work, to include an *explicit discussion of the anchor system's role in ensuring the integrity of the bridge beam*, including the loading on the abutments.

Damping contribution on horizontal motion and bending moment about strong axis are strongly dependent on drag coefficients of the mooring lines. The figure below indicates that the mooring damping significantly reduces the (low frequency) horizontal motions of the anchored pontoons [7].

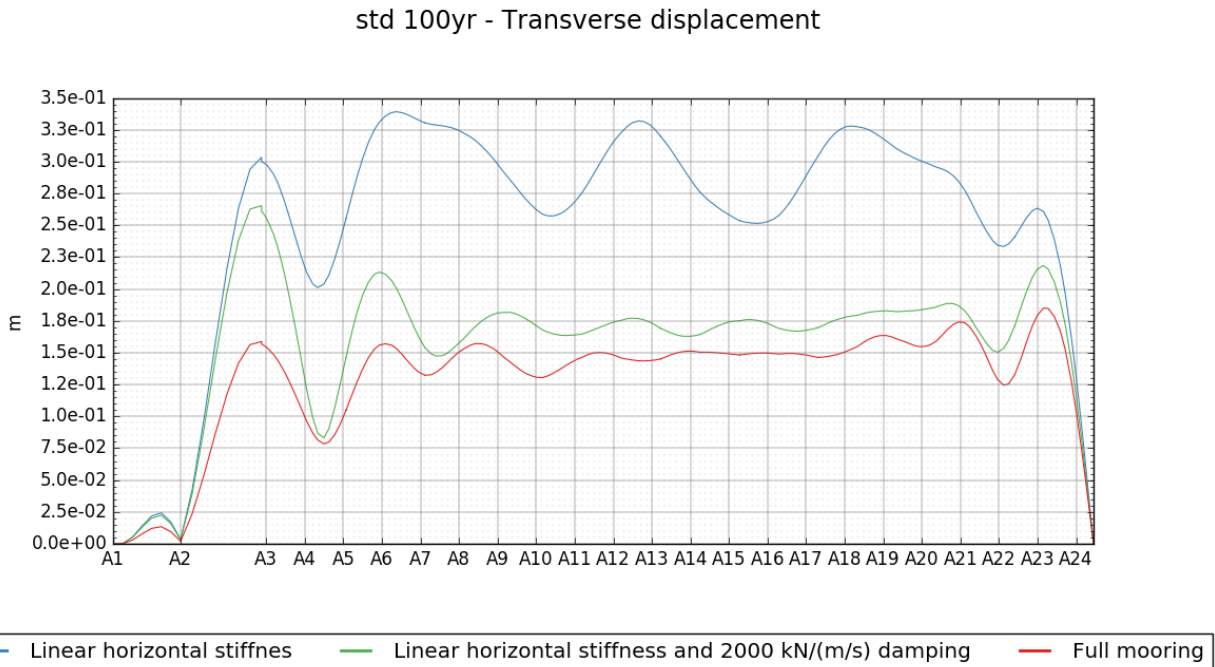


Figure 19 Standard deviation of transverse displacement of the straight bridge with no mooring damping, applied linear damping and drag damping from full mooring line model, taken from [7]. NB! Pontoon distance 200 m

This is also stated in the 'Robustness and sensitivity analysis', [7], Section 8.1:

"More work needs to be done to fully understand the behaviour of the mooring system and the relationship between the modal shapes in the bridge structure and the mooring stiffness and damping. The coupled problem between the bridge structure and mooring system are an interesting case to be studied in a model test."

In the independent analysis by DNV-GL [20] the drag coefficients for the mooring lines are based on DNVGL-OS-E301, and the used coefficients can be taken as upper limit for mooring design. This is also the value that has been used for design analyses. A sensitivity with zero drag coefficients has also been analysed. The appropriate coefficients for bridge design may be lower than the coefficients from DNVGL-OS-E301. This should be studied in future phases.

Comprehensive reference to existing rules and guidelines regarding the safety of offshore mooring systems are included in the design basis, [17]. The majority of these references deals with the problem of mooring one rigid floating body of a 6 DOF force vector due to wind, waves and current, with fairly wide motion tolerances. In the present case there is a large number of rigid bodies interconnected by an elastic beam, and four of the bodies (pontoons) are in addition restrained by several mooring lines. The motion tolerances will differ along the bridge beam; wider in the midspan than near the ends. The established practice with regard to accidental environmental loading and damage conditions (line failures) is probably not sufficient here.

4.9 Measurements and validation of response calculations

4.9.1 Wave response

Kvåle and Øiseth [30] compared measured bridge pontoon accelerations for Bergsøysundet floating bridge to numerical predictions based on wave spectra fitted to measured waves. The comparison was done for one specific case, applying a frequency domain method with first order waves to predict the response. They found good agreement between the measurements of lateral responses, decent agreement for the vertical response and poor agreement (consistent underestimation) for the torsional response.

4.9.2 Wind response

In general, there seems to be few validation studies of wind forces on bridges. The few that exist compare only for limited periods of time [26]. Numerical simulations of wind induced response was performed for the Lysefjord bridge, and compared to mid-span acceleration measurements [26]:

The increasing discrepancy between computed and measured buffeting responses suggests that a customized wind turbulence model should be proposed for such complex terrain topography that involves narrow fjords, mountains and an island. Most importantly, it indicates that the terrain category should be carefully chosen for the design of future fjord-crossing bridges, where wind direction will also be an important factor in determining the correct terrain category, as seen in the Lysefjord Bridge case.

As described by Fenerci et. al. ([28] and [29]), a measurement campaign on the Hardanger bridge (suspension bridge), between 2013 and 2016, showed larger measured accelerations than predicted by numerical model. These accelerations were closely correlated with the measured wind speed variability, which showed strong dependency of wind direction and surrounding terrain.

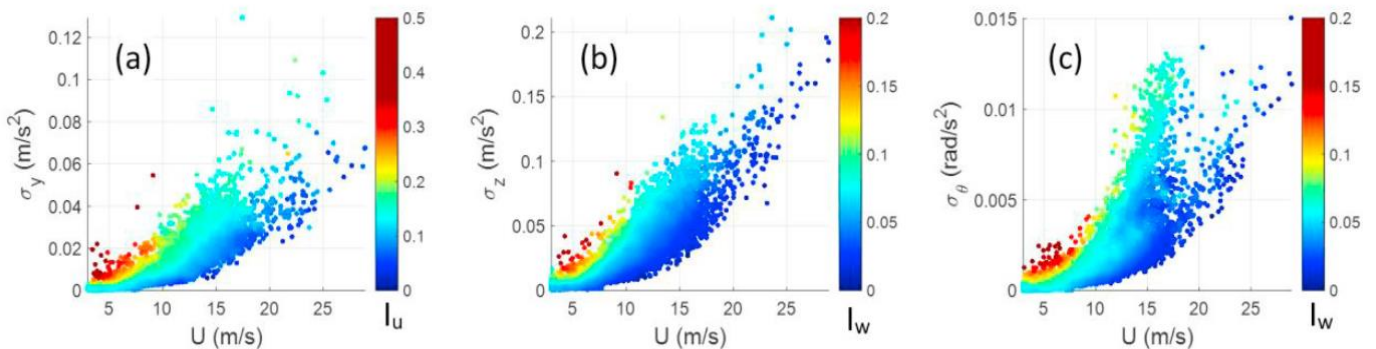


Figure 20 RMS of measured acceleration response vs mean wind speed and turbulence intensity (I_u , I_w , I_w) for lateral (a), vertical (b) and torsional (c) response of the Hardanger bridge girder [28].

In a study by Fenerci and Øiset [29], the bridge girder response of the Hardanger bridge was predicted using a frequency domain model and buffeting theory and compared to measurements. This study supports the conclusions drawn in Fenerci et. al. [26] and Wang et. al. [28], that the design wind field description is not sufficient to be able to predict the correct responses. Hence, refined models seem to be required in order to achieve a proper representation of the wind velocity and wind load components. It was also indicated that the lateral response of the bridge girder was influenced by the wind loads which are acting on the cables, and that this is something that should be carefully considered in modelling.

These studies suggest that validation of numerical models and load calculation methods should be done with numerical wind fields that are generated based on on-site measurements, that consider the surrounding terrain and wind direction.

4.10 Design criteria, limit states and response

In the following, the design criteria and the corresponding mechanical limit states are first summarized. Subsequently load effect combinations are considered together with the respective codified design checks to be performed.

4.10.1 Design criteria and limit states

The design criteria for different bridge components generally correspond to by mechanical limit states which are formulated in terms of functions which involve relevant load effects and capacity parameters. Here, we focus on limit states for the low bridge, i.e. the part of the bridge that constitutes the main span. First the Ultimate Limit States (ULS) are considered, which correspond to von Mises yielding in addition to local buckling of stiffened panels and global buckling of bridge segment. The design criterion associated with this limit state is usually formulated in terms of a nominal yield stress. It should also be kept in mind that initial yielding by itself is not a physical failure mode. However, yielding of large parts of the cross-section and possibly full plastification will generally lead to residual bridge deformations which represent physical failure conditions.

For design of cable-stayed bridges, aerodynamic stability also needs to be verified, similar to the design of suspension bridges. However, this limit state is presently not relevant for the low bridge.

Having considered the ULS Limit States below, the Fatigue Limit State (FLS) is addressed followed by the Serviceability Limit State (SLS) and the Accidental Limit State (ALS). For the latter, design criteria are also considered which involve environmental loads with much longer return periods than for the ULS Limit State.

ULS - Von Mises Yielding

For the low bridge, the von Mises stress is checked at 5 points around the cross-section of the bridge girder as shown in the figure below (based on nominal stresses). The highest von Mises stress seems to occur at point 3 in this figure, somewhat depending on whether shear leg effects are considered or not.

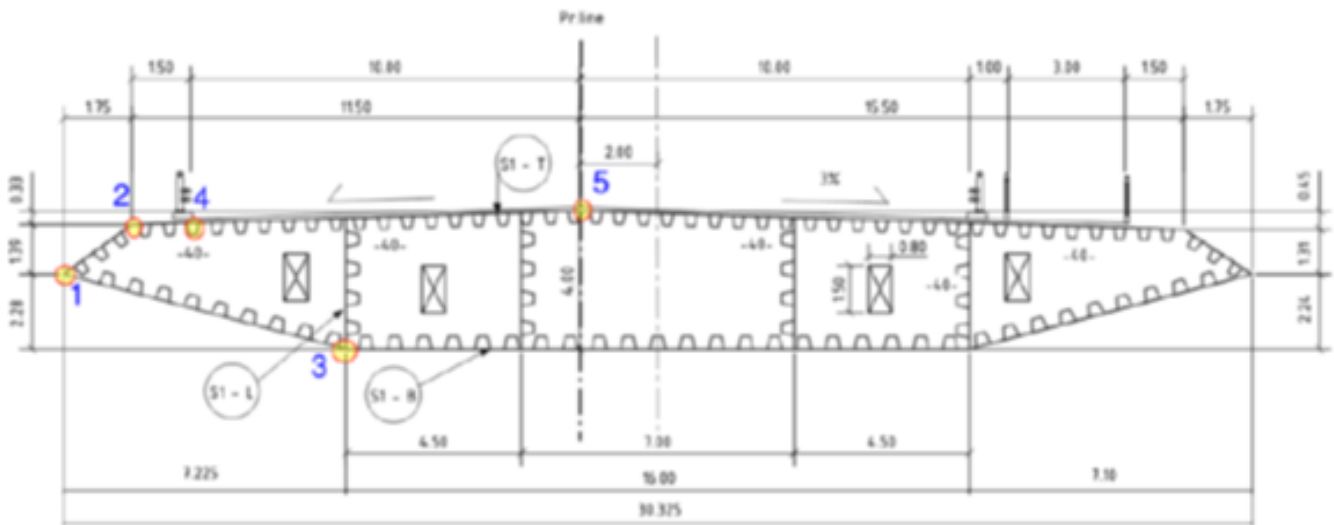


Figure 7-4 Stress points at Section type S1

Figure 21 Points around the cross-section where von Mises stresses are checked, from [18].

ULS - Local buckling of stiffened panels

Local buckling of the stiffened panels is checked based on DNVGL-RP-C201: "Buckling Strength of Plated Structures, October 2010, [21]. In the design check, three different types of stiffeners were considered.

ULS - Global buckling (including short term dynamic extremes)

Regarding global buckling of "sub-sections" (i.e. segments of the bridge), this may occur e.g. due to the combined static and dynamic axial force becoming negative (i.e. compressive). This may take place for a short period of time and may be critical for integrity of the bridge girder. The following quote (from a memo issued by NTNU on instability phenomena for floating bridges, [39]) is reproduced here:

One of the great challenges that needs to be addressed is the fact that it is not easy to determine whether a system subjected to stochastic loading is stable or not from just looking at the response. The system might for instance be unstable for only a relatively short time period, which might not result in a very severe dynamic response in the particular simulation carried out, but that can give a very severe dynamic response if the period last longer or combinations of response and load effects are more unfavourable. One of the objectives of any design is to document that dynamic effects including resonances, parametric excitation, parametric resonances, aeroelastic instabilities are controlled and accounted for and that the bridge is stable.

This limit state is not considered in more detail in the present document.

FLS - Fatigue damage accumulation

Fatigue damage due to the local stresses caused by traffic loads are analyzed in [23]. The magnitudes of the cyclic local stresses imply that the fatigue damage is too high such that the deck plate is too thin. The details of the stiffener to cross-beam connection also need to be improved.

For the stresses due to the combined effect of tidal variations and traffic load at the northern end span is larger the allowed value mainly due to shear lag effects.

For stresses caused by environmental loads (e.g. wind, wave) the fatigue damage is unacceptable for cross-sections where large shear lag effects are present. By modifying the bridge cross-section such that shear-lag effects on the stress components are minimized this fatigue damage contribution can be reduced to an acceptable level.

Furthermore, if the thickness of the plate in the bridge deck is sufficiently increased the fatigue damage caused by the combined cyclic stress effects due to tidal, traffic and environmental loads can be adequately reduced. However, in the report the following is emphasized (quote):

It is found in the analyses carried out that the fatigue damage calculated is sensitive to the assumptions made and that the combination of fatigue damage from various sources add the complexity and consequently the accuracy of the calculations.

Design with respect to the Fatigue Limit State is presently based on the SN-formulation. The value of the fatigue safety factor which is applied in the analysis will correspond to the material safety factor (i.e. 1.35, see the Table below) taken to the power of the SN-curve exponent (i.e. $m=3$ possibly combined with $m=5$ for a high number of cycles). This implies that the resulting “effective safety factor” will vary for different SN-curves with different stress exponents.

SLS - Serviceability criteria (static and dynamic response criteria: deformations and accelerations)

Serviceability criteria are associated with acceptable limits of displacements, velocities and accelerations which relate to driver safety, comfort criteria etc.

ALS - Accidental limit state criteria: Plastic deformations, fracture

An important accidental load is due to collision of a ship with the bridge. Specialized case studies have been performed to design against this type of loading.

Accidental conditions which correspond to environmental loads with much higher return periods than for the ULS limit states are also to be considered (i.e. with return periods of 10 000 years).

4.10.2 Characteristic load calculation

For ULS the characteristic response applied for engineering design is taken as the 90% fractile maximum from ten 1-hour realisations, for SLS the 50% fractile from and for ALS the 95% fractile. The fractiles are found by a Gumbel-fit of the maximums from the realisations. Regarding the simulation time applied for each simulation (i.e. 1 hour), the inherent statistical uncertainty associated with estimation of extreme response levels is likely to be on the high side.

In any case, having ten realisations of such 1-hour simulations available allows the corresponding standard deviation (or equivalently the variance) of this extreme response to be estimated. The percentage uncertainty (i.e. the ratio between the standard deviation and the mean value of the estimated extreme value in percent) can then also be computed. Furthermore, this allows prediction of the corresponding extreme response uncertainty for increasing simulation lengths to be made.

4.10.3 Load combination

The aim of combining responses due to different sources of loading is to obtain a characteristic total response where the probability of exceedance is a certain value determined by the safety class of the structure or structural part. The characteristic response can normally be obtained for several different combinations of permanent loads, traffic loads and environmental loads.

A second type of load combination arises at the cross-section level at which the maximum values of the stress components (e.g. axial stress, bending stresses and torsion stresses) do not necessarily occur at the same point in time due to phase differences between response of the structure for different natural modes.

Regarding the first type of load combinations, three different Ultimate Limit State (ULS) conditions are considered for the Bjørnafjorden bridge concepts. These are the following, see e.g. [18]:

- **ULS 1: Dominating permanent load.** The traffic load is combined with 1-year extreme environmental load
- **ULS 2: Dominating traffic.** The traffic load is combined with 1-year extreme environmental load. A different set of combination factors than those considered for the ULS1 condition is applied.
- **ULS 3: Dominating environmental load.** Environmental loads with 100-year return period.

The ULS3 condition is further split into four different sub-categories. These correspond to different combinations of wave and wind excitations (as represented by their respective characteristic parameters, i.e. wind velocity and direction, wave sea state parameters and direction, current magnitude and direction). A summary of the four load conditions is provided in the table below (i.e. Table 3-24 in [18]).

Table 9 ULS design load cases for wind, waves and current corresponding to 100 year environmental conditions, from [18].

Table 3-24 Design load cases for wind, waves and current for 100y environmental conditions

Load case	100-y wind		100-y wind sea		100-y swell sea			100-y current		
	Wind vel.* [m/s]	Dir. [deg]	H _s [m]	T _p [s]	Dir. [deg]	H _s [m]	T _p [s]	Dir. [deg]	Curr. vel. [m/s]	Dir. [deg]
ULS_100y_1	25.1	100	2.8	6.6	90	-	-	-	1.4	100
ULS_100y_2	25.1	100	2.8	6.6	75	-	-	-	1.4	100
ULS_100y_3	29.5	280	2.5	6.2	335	0.4	20	300	1.4	280
ULS_100y_4	29.5	280	2.4	5.9	280	0.4	20	300	1.4	280

* This is the 10min mean wind speed 10m above sea level. This is however applied stationary for 3 hours in our calculations.

The aim of combining responses to environmental actions is to obtain a characteristic total response where the probability of exceedance is a certain value determined by the safety class of the structure or structural part. The characteristic response can normally be obtained for several different combinations of environmental actions (as for the present case of the Bjørnafjorden crossing).

For the side-anchored bridge, ULS 3 is found to be the governing load combination. Some further observations related to the relative magnitude of load effects due to the different sources are summarized below with focus on the girder for the low bridge (i.e. the floating main span of the bridge). These results are based on the analyses performed in [3].

The partial coefficients which are applied for the different types of load components are given in Table 3 below. We see that for the environmental loads the partial coefficient (i.e. load factor) is as high as 1.6.

If the ALS instead of the ULS limit states are considered, the load return periods are 10 000 years instead of 100 years. Furthermore, the partial coefficients for the loads are typically set to 1.0.

Table 10 Partial coefficients for different types of load components, [18].

Table 7-1 Load factors

Load	Load factor
Permanent loads	1.2
Environmental loads without traffic	1.6
Storm surge	1.6
Tide	1.1

The corresponding partial coefficient for the material resistance is given in Table 4 and is equal to 1.1.

Table 11 Partial coefficient for material resistance, [18].

Table 7-2 Material factors

Limit state	Material factor
Ultimate strength	1.1
Fatigue	1.35

According to [3], for the top-flange in the bridge girder the ULS 3 condition governs the design with dominating strong axis moments from waves. The main wave case is from the east sector (75 deg), which is the sector that corresponds to the largest wave heights and longest peak periods. The wind loading is significantly larger from the west sector, but the strong axis moment from the dynamic wind is significantly dampened by the mooring system. Accordingly, the strong axis moment response is dominated by wave action. The relative magnitudes of the different load effects are shown in the Figure below for the top flange.

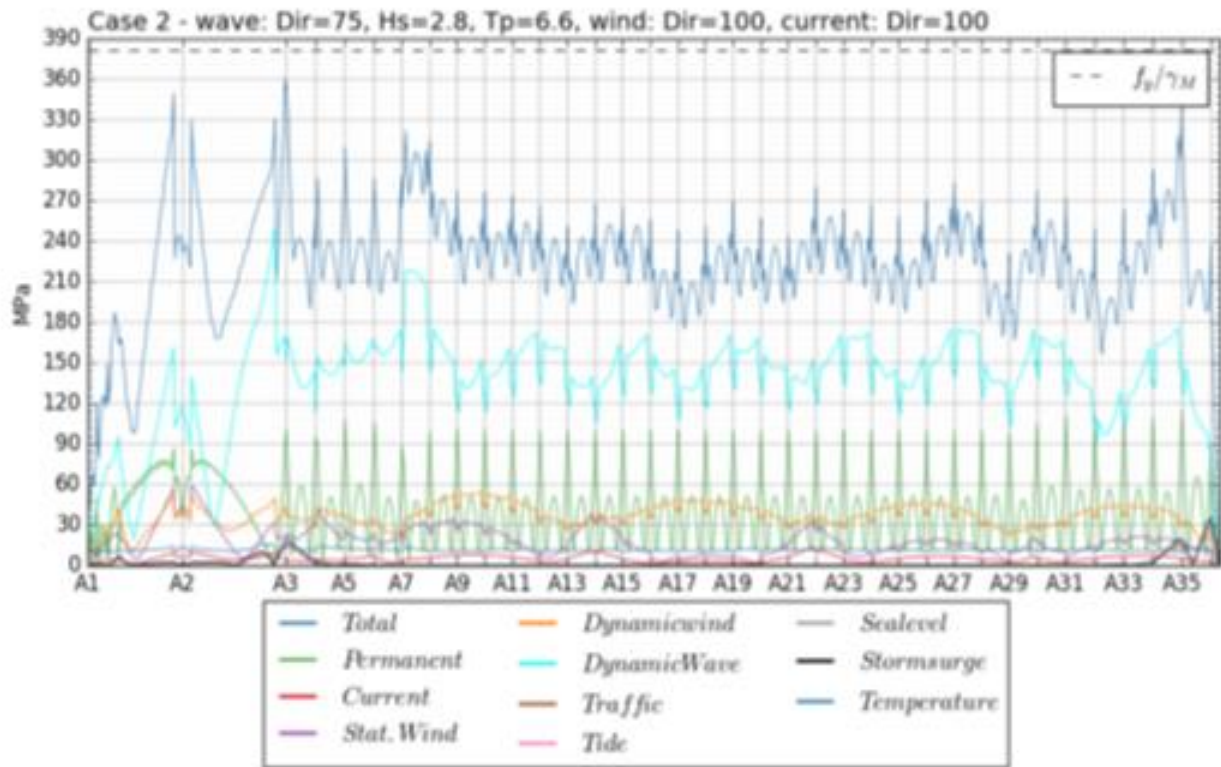


Figure 11-18: Break-down of the load contributions for the ULS3 load combination in the top flange. Note that traffic loads are not included for this load combination, even though it is labelled in the legend.

Figure 22 Contributions from different load effects for the straight bridge (with shear leg effects included) corresponding to the ULS 3 load combination in the top flange of the bridge girder, from [5].

For the bottom flange, the stress is dominated by weak axis bending moment from the ULS 2 (dominating traffic loading combined with 1-year environmental loads) and ULS 3 (100-year environmental loads with no traffic). The contributions from the different load effects for the ULS 2 case is shown in Figure 23 and for the ULS 3 case in Figure 24, from [3].

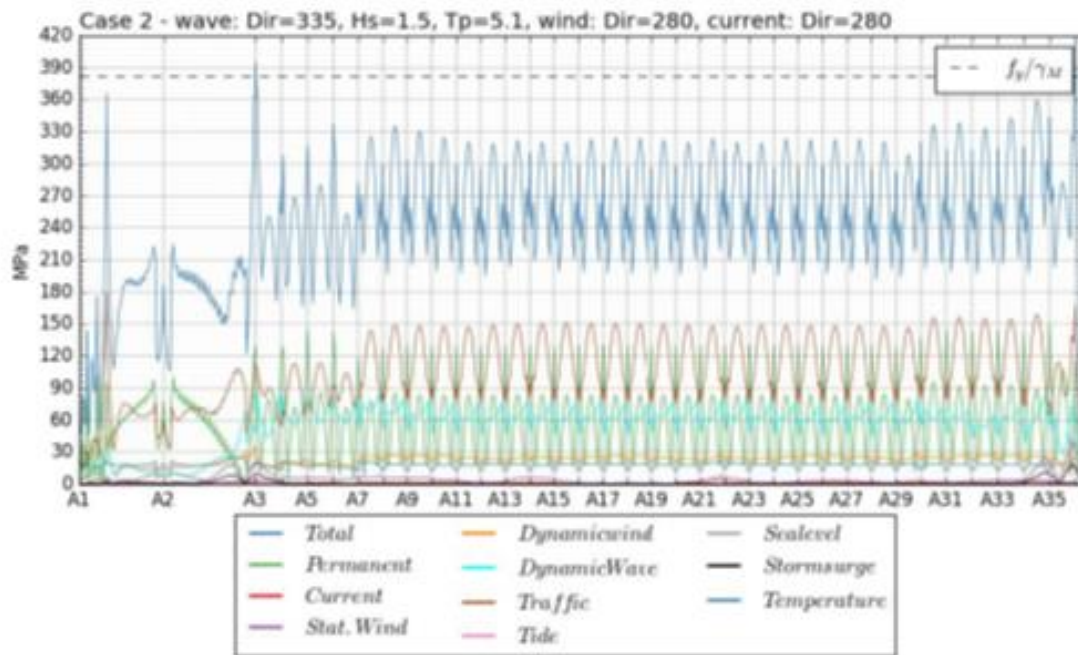


Figure 11-23: Break-down of the load contributions for the ULS2 load combination in the bottom flange for the 1-year environmental case 2.

Figure 23 Contributions from different load effects for the straight bridge (with shear leg effects included) corresponding to the ULS 2 load combination in the bottom flange of the bridge girder, [3].

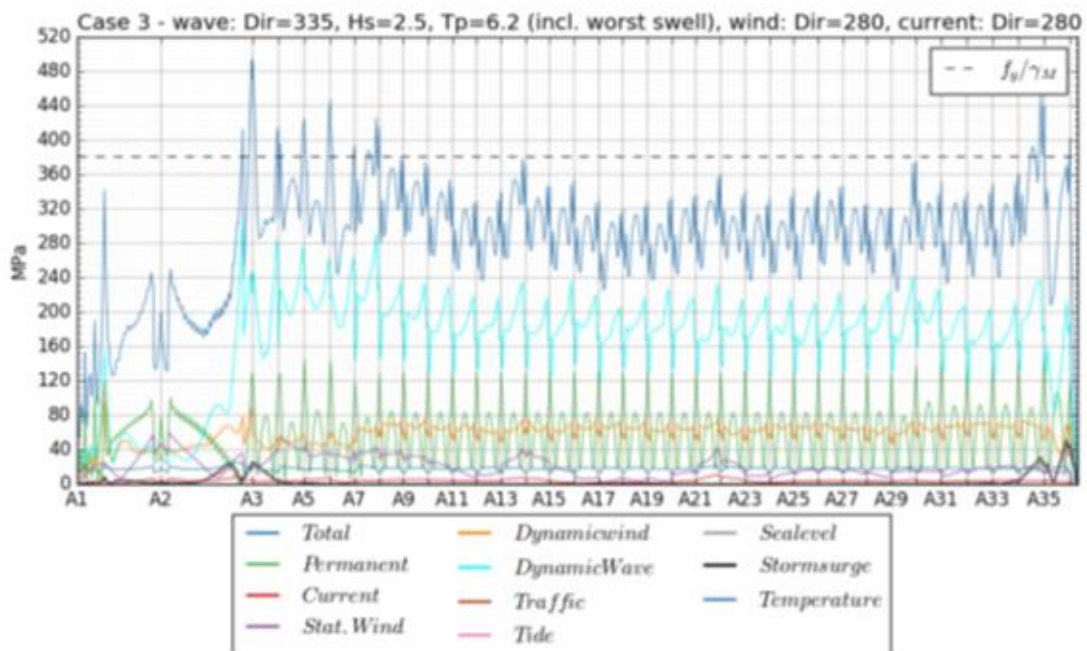


Figure 11-24: Break-down of the load contributions for the ULS3 load combination in the bottom flange for the 100-year environmental case 3. Note that traffic loads are not included for this load combination, even though it is labelled in the legend. For discussion of the local exceedance, see section 13.4.3.

Figure 24 Contributions from different load effects for the straight bridge (with shear leg effects included) corresponding to the ULS 3 load combination in the bottom flange of the bridge girder, [3].

For the assessment of extreme responses needed in design of marine structures, a full long-term analysis is the most accurate approach. In the long-term approach, short-term structural response analyses have to be carried out for a very large number of combinations of the environmental parameters, whether full integration or Monte Carlo simulation is used. For complex structures, the computational effort is often considered to increase above acceptable levels.

The computational effort of long-term extreme response analysis can be reduced either by reducing the computational effort of the short-term analyses, or by developing methods that require less short-term analyses in the computation of the long-term response. The so-called contour line methods belong to this second category. Each “point” along the contour represents an extreme environmental condition corresponding to a given return period (e.g. 100 years) for which a response analysis is to be performed. The highest response level for a sequence of such points is then assumed to be the extreme response with the given return period. Application of this procedure to floating bridges was studied by Giske et. al. [37,38] and was found to give significant savings in terms of computation time.

Another important issue with respect to load combinations is how to combine short term extreme values of the dynamic load effects. Two methods have been applied in [5]:

- Determine the characteristic response of the individual load components (i.e. dynamic wind, dynamic wave, static wind current and mean drift) separately, and assume that the combination factors account for the correlation between stochastic load groups and load components.
- Statistic estimate from all realisations of the different load components to verify that the above assumption is conservative.

The bridge girder loads were mainly governed by the combination with dominating environmental loads.

To perform an adequate calibration of design formats and safety factors for ultra-long span floating bridges, a full probabilistic modelling of all relevant sources of variability and the associated uncertainties will be required. Having established such probabilistic models, structural reliability analysis can be carried out and the corresponding failure probabilities for relevant mechanical limit states can be calculated. Comparing these probabilities with target values, the engineering design formats that are required to meet these targets can be identified.

Such a complete reliability analysis represents a very comprehensive task both in terms of research efforts and computational resources. It is still believed that this topic needs to be addressed as part of future research efforts. Clearly, there are still a number of studies that are first required in order to characterize the model uncertainties associated with the load representation, numerical structural model and response analysis in an adequate manner.

4.10.4 Design principles and critical response components

The following design principles for the pontoons were applied in [5]:

- *Controlling the weak axis eigenmodes and resonances through adding sufficient large bottom flange of the pontoon to gain enough heave added mass to lift the eigenperiods out of the wind driven domain.*

- Control the lengths of the pontoon to allow cancellation of the Froude-Kriloff pressure at the front and back ends. I.e. the pontoon should have lengths close to the critical wave lengths in the wind spectrum with the highest energy. In our case here for waves with periods around 6.6s.
- Control the geometry such that there is a phase distribution of the force in the length direction of the pontoon, this is best achieved by using a diamond shaped pontoon.

Bjørnafjorden straight bridge mooring: Taut-semi-taut with bottom chain, wire and top chain. No line on the bottom in the static condition. Varying mooring configuration because of uneven seabed and seabed conditions. Analysed with intact and with line failure (ALS).

4.10.5 Observations from design checks

In [18], the following observations are made based on the design checks which were performed:

The results of the ULS analyses and capacity checks presented in Section 7.5, 7.6 and 7.7 shows utilisation above 1 for both buckling and yield. In general, the highest utilisations are seen for transitions in cross-section from type F1 to S1 for the low bridge and H1 to F3 for the low bridge. The main reason for the high utilisation is that the Fx type of cross-sections are not fully effective against weak axis bending due to shear lag effects. Thus, it is recommended that all the cross-sections are designed with sufficient number of longitudinal webs in order to obtain a fully effective cross-section. This will reduce the normal stresses with a factor of 1.5 to 2 at the worst locations. In addition, the introduction of additional webs will increase the shear area and thus reduce the shear stress.

Assuming the same cross-sectional properties but neglecting shear lag reduction it is only the buckling check of stiffeners at the bottom flange that is not meeting the requirements. This will be valid for several positions along the bridge.

In the high bridge the too high stresses are calculated close to axis 3. Both yield checks and buckling checks will fail to meet the criteria.

Accordingly, it is found that for the straight bridge concept both yielding and (stiffened) plate buckling are critical ultimate limit states. The importance of including shear lag effects for calculation of stresses is also clearly illustrated.

In [18] it is also observed that the amount of additional steel material which is required in order to meet the ULS design criteria is very modest provided that the most important strength components are selected for upgrading.

In relation to the FLS design criteria, it was found that for stresses caused by environmental loads (e.g. wind, wave) the fatigue damage is unacceptable for cross-sections where large shear lag effects are present. By modifying the bridge cross-section such that shear-lag effects are minimized this fatigue damage contribution can be reduced to an acceptable level.

Furthermore, if the thickness of the plate in the bridge deck is sufficiently increased the fatigue damage caused by the combined cyclic stress effects due to tidal, traffic and environmental loads can be adequately reduced.

From the above observations, it is clearly seen that accounting for shear lag effects in the stress analysis is important as part of adequate limit state design procedures for the ULS.

5 Identification of Gaps

The following gaps are listed in conceptual groups according to the table label but are otherwise non-prioritized and non-structured.

5.1 Uncertainties and gaps in Design Methods (related directly to WP3 and WP4)

Table 12 Uncertainties and gaps in design method.

Knowledge gap	Actions required to close gap (sensitivity studies, method development, numerical tool development, model tests, full scale measurements)
Correlation basis for combination of environmental loads due to different sources in calculation of characteristic structural response (section forces)	Reliability analysis.
Criteria for occurrence of global dynamic buckling (of curved bridges)	Development of engineering models. <i>(Outside of scope for LFCS.)</i>
Shear lag effect in global response analysis	Incorporation of shear lag effect in global analysis; <ul style="list-style-type: none"> • Redesign • Account for shear lag <i>(Outside of scope for LFCS.)</i>
Interaction effects between wind, wave and current loads	Numerical sensitivity studies.
Mooring system functional requirements beyond mandatory requirements, i.e. to reduce response	Discussion of the anchor system's role in ensuring satisfactory bridge response.
Mooring system damping effects on response	Numerical sensitivity studies and hydrodynamic model tests.
Mooring system influence on mode shapes and dynamic behaviour of the bridge	Numerical sensitivity studies.
Response after line failure(s) possible implication on design	Study on mooring line system effects
Complex numerical models for response analysis.	Establish best practice for modelling of floating bridges.
Uncertainty in extreme value calculation [$X_{max} = k \cdot \sigma$, where k is a response gust factor] <ul style="list-style-type: none"> • Gaussian • Non-Gaussian 	Uncertainty analysis and assessment of necessary simulation length and number of random realizations.
Characteristic environmental condition; wind (10 min.), wave (3 hours), current - to 1 hour response timeseries	1): Environmental condition: compare averages based on gust (3 sec), 10 min wind, 60 min wind 2): Perform response analysis to show the effects.
Mooring system design rules and safety factors for 100-year design life	Reliability analysis. <i>(Outside of scope for LFCS.)</i>

5.2 Uncertainties and Gaps Related to Environmental Description (WP1)

Table 13 Uncertainties and gaps related to environmental description.

Knowledge gap	Actions required to close gap (sensitivity studies, method development, numerical tool development, model tests, full scale measurements)
Effects of inhomogeneous wave conditions	Develop method to describe inhomogeneous wave fields numerically and perform numerical simulations of response to these.
Effects of inhomogeneous wind field	Develop method to describe inhomogeneous wind fields numerically and perform numerical simulations of response to these.
Low frequency response to unknown low frequency content in wind spectra	Uncertainty of low frequency content of spectra should be assessed. Spectra should be chosen carefully before applied in numerical case studies.
Response to increased vertical wind turbulence due to wave.	1): The effect on turbulence due to wave height and distance from girder to mean water level is to be assessed by lab experiments or CFD 2): Perform numerical case studies.' (<i>Outside of scope for LFCS.</i>)
Superposition of low frequency response to wind sea and swell wave	Case studies applying separate and combined spectra.

5.3 Uncertainties and Gaps Related to Loads (WP2)

Table 14 Uncertainties and gaps related to loads.

Knowledge gap	Actions required to close gap (sensitivity studies, method development, numerical tool development, model tests, full scale measurements)
Effect on global response of hydrodynamic interaction between columns.	Hydrodynamic experiments and investigations with full numerical model.
Validity of Newman's approximation	Hydrodynamic experiments.
Effect of QTF obtained with correct first order wave response.	Iterative numerical studies.
Interaction effects between wind, wave and current loads	Numerical simulations.
Buffeting theory vs. quasi-steady non-linear wind loads	Comparison of results from numerical model using both models.
Validation of wind induced global response	Full scale measurements.
Inclusion of transverse motion in flutter analysis.	Methodology and tool development.

5.4 Uncertainties and Gaps Related to Model Tests (WP5)

Table 15 Uncertainties and gaps related to model tests.

Knowledge gap	Actions required to close gap (sensitivity studies, method development, numerical tool development, model tests, full scale measurements)
Effect on global response of hydrodynamic interaction between pontoons.	1): Numerical analyses for experimental studies 2): Hydrodynamic experiments including multiple pontoons 3): Perform global numerical analyses to compare with 2).
Effects of inhomogeneous wave conditions	Experiments with inhomogeneous wave conditions
Uncertainty in truncated bridge modelling for model tests	Investigate implications by numerical model of truncated model.
Difference frequency wave response.	Hydrodynamic experiments with low frequency modes represented in the model.
Influence of viscous effects on the pontoons, on the first and second order responses.	Hydrodynamic experiments.
Inclusion of wind in hydrodynamic tests	Establish an approach for including wind action in hydrodynamic model test.

5.5 Limitations in Software

Table 16 Limitations in software.

Knowledge gap	Actions required to close gap (sensitivity studies, method development, numerical tool development, model tests, full scale measurements)
Numerical inhomogeneous wave field description	Implement in SIMO/RIFLEX (a stand-alone tool to pre-generate wave forces or as wave field description in the code).
Inhomogeneous wind field in SIMO/RIFLEX	Develop turbulence generator with inhomogeneous conditions.
Wind field with adaptive grid for long bridges	Develop grid generator.
Frequency-dependent aerodynamic properties in time domain simulations	Implement state-space model for wind loads. Input from already performed wind tunnel tests for the testing of the state-space modelling. <i>(Outside of scope for LFCS to perform new wind tunnel tests.)</i>
Numerical models for response analysis are large and complex	Benchmarking studies and instruction manuals (for modelling [structure, mass, damping], execution of analysis, sample size, etc.) specially written for floating bridges.
Hydrodynamic interaction matrices in global response analysis (numerical tool gap)	Implement in SIMO/RIFLEX (for required number of pontoons based on interaction effect; any software limitation?)
Linear analysis in hydrodynamic analysis solvers	Implement linear solvers and eigenvalue solvers considering frequency dependent added mass and damping.

6 Recommendations

6.1 Work package 3 and 4 connections to other work packages

Several uncertainties that are relevant for response calculations (section forces) were identified in the review. Some of the actions required to close these gaps are covered by other work packages. The recommendations in this section concern the uncertainties that are directly related to response of the bridge and mooring lines. Some studies depend on environment and load input from WP1 and WP2. Other studies provide the basis for hydrodynamic testing in WP5.

Table 17 Gap / action dependencies between work packages.

Item	Method	Dependency
Inhomogeneous wave description	Method development	WP1
Inhomogeneous wind field description	Method development	WP1
Numerical wave field description	Software development	WP1
Numerical wind field description suited for long bridge	Software development	WP1
Full QTF accounting for correct first order motion	Numerical study	WP2
Full QTF vs. Newman's approximation	Numerical study	WP2
Buffeting load model in SIMO/RIFLEX	Software development	WP2
Viscous forces		WP2/WP5
Wave drift damping		WP2/WP5
Hydrodynamic interaction in coupled SIMO/RIFLEX	Plans for implementation MPFS	

6.2 Scope for Methodology Development for WP3 and WP4

Methods to evaluate global dynamic buckling are specific to the curved bridge, and also the topic is covered by other projects. Thus, this topic is out of scope. Aerodynamic instabilities are also considered to be out of scope for this project.

Table 18 Scope for methodology development for WP3 and WP4.

Item	Description
Shear lag effect in global response analysis	Discuss and propose method to include bridge girder stiffness accounting for shear lag: design to limit shear lag or accounting for shear lag. <i>Out of scope for LFCS.</i>
Model truncation study	Compare a numerical model of the entire bridge length to a model with reduced length; investigate limitations of the reduced length model to be used in hydrodynamic model tests. Find reasonable boundary conditions for the reduced model tests.
Estimating uncertainty in extreme response predictions	Calculate long term response characteristics of response to inhomogeneous conditions and compare with results from simplified methods. Compare results from various simplified extreme response estimation methods toward long-term extreme response.

6.3 Scope for Case Studies for WP3 and WP4 (models, generic, etc.)

Table 19 Scope for case studies for WP3 and WP4.

Item	Description
Response to inhomogeneous waves	Assess response to inhomogeneous wave field. Compare with homogenous waves.
Response to inhomogeneous wind	Assess response to inhomogeneous wind field. Compare with homogenous wind.
Combination of environmental load effects	Compare methods for combination of environmental load effects from different environmental loads as well as combination of different cross-section forces; static, dynamic, extreme.
Buffeting theory vs. quasi-steady non-linear theory	Compare the responses for two different approaches.
Interaction effect between wave and wind loads	Investigate the implications of superposition of wind and wave load effects.
Hydrodynamic interaction between pontoons	Effect of diffraction and added mass considering interaction between pontoons on full model in short-crested irregular sea. Compare to model with no interaction.
Validity of Newman's approximation	Compare slow drift response calculated by Newman's approximation to response with full QTFs calculated for a flexible structure.
Effect of limited number of actuators	For model tests, investigate the implications of reduced number of degrees of freedom for actuation of wind loads in hydrodynamic model tests.
Mooring system damping	Numerical sensitivity study of mooring system damping.
Tuning of numerical model to hydrodynamic experiments	Full scale numerical model with hydrodynamic coefficients tuned to model tests.
Sensitivity to low frequency content in wind spectrum	Simulation of full bridge model with wind loads from spectrum based on measurements.
Validation of wind response analysis methods against full scale measurements	<i>Out of scope for LFCS</i>
Validation of wave response analysis methods against full scale measurements	<i>Out of scope for LFCS</i>
Dynamic stability of curved bridge girder	<i>Out of scope for LFCS</i>
Aerodynamic instability in time domain	<i>Out of scope for LFCS</i>

6.4 Scope for software improvement

Table 20 Scope for software improvement.

Item	Description
Inhomogeneous wave field for numerical models (linked to WP1 and WP2)	<p>Step 1: Develop code to pre-calculate wave forces based on an inhomogeneous wave field that can be used in response analysis. <i>Stand-alone general module.</i></p> <p>Step 2: Implement inhomogeneous wave field in SIMO to allow for hydroelastic analysis. <i>SIMO-RIFLEX.</i></p>
Inhomogeneous wind field for numerical models (linked to WP1)	<p>Step 1: Develop grid generator with nodes at relevant bridge locations. Step 2: Develop tool to generate inhomogeneous wind field in the grid in Step 1. <i>Stand-alone general module(s), Step 1 and Step 2.</i></p>
Frequency dependent aerodynamic derivatives in time domain aeroelastic code (linked to WP2)	<p>Develop external dynamic linked library (DLL) to RIFLEX that calculated aeroelastic forces based on frequency dependent aerodynamic derivatives using state-space formulation. <i>SIMO-RIFLEX, however, the DLL may be applied towards other codes as well.</i></p>
Hydrodynamic coupling in coupled SIMO-RIFLEX simulation	<p>Implement hydrodynamic added mass between bodies (non-diagonal terms). Already available in SIMO but not in the coupled simulation. <i>(MPFS-Singapore proj. financed; MPFS-LFCS cooperation.)</i> <i>SIMO-RIFLEX.</i></p>
Linear solver in coupled simulation (SIMO/RIFLEX)	<p>Implement option for applying constant mass-, damping- and stiffness matrices in coupled simulation. Simulation time reduction of a factor of 6-7. <i>(MPFS-Singapore proj. financed; MPFS-LFCS cooperation.)</i> <i>SIMO-RIFLEX.</i></p>

7 References

7.1 General

- [1] Håndbok-N400 Bruprosjektering
- [2] Einar Strømmen, Theory of bridge aerodynamics, Springer, 2006

7.2 Bjørnafjorden Crossing

- [3] Statens Vegvesen, SBJ-32-C3-SVV-90-BA-001, Design basis Bjørnafjorden floating bridges, Rev C, 07.03.2017
- [4] Statens Vegvesen, SBJ-31-C3-MUL-22-RE-100, Analysis and design (Base Case)
- [5] Statens Vegvesen, SBJ-30-C3-NOR-RE-102, K7 Bjørnafjorden end-anchored floating bridge – Global analyses summary.
- [6] Statens Vegvesen, SBT-PGR-RE-211-011, K1 & K2 Design Summary
- [7] Statens Vegvesen, SBJ-31-C3-MUL-22-RE-104 Analysis and design, Appendix D Robustness and sensitivity analyses, 19.05.2017
- [8] Statens Vegvesen, NOT-KTEKA-021, Curved bridge south, summary of analyses, V1.0, 15.02.2016
- [9] Zhengshun Cheng, Zhen Gao, and Torgeir Moan. "Hydrodynamic load modeling and analysis of a floating bridge in homogeneous wave conditions." *Marine Structures* 59 (2018): 122-141.
- [10] Zhengshun Cheng, Zhen Gao, and Torgeir Moan. "Wave load effect analysis of a floating bridge in a fjord considering inhomogeneous wave conditions." *Engineering Structures* 163 (2018): 197-214.
- [11] Zhengshun Cheng, Zhen Gao, and Torgeir Moan. "Numerical modelling and dynamic analysis of a floating bridge subjected to wind, wave and current loads" *Journal of Offshore Mechanics and Arctic Engineering* 141 (2018), Accepted manuscript June 05.
- [12] Yuwang Xu, Ole Øiseth, and Torgeir Moan. "Time domain modelling of frequency dependent wind and wave forces on a three-span suspension bridge with two floating pylons using state space models." *ASME 2017 36th International Conference on Ocean, Offshore and Arctic Engineering*. American Society of Mechanical Engineers, 2017.
- [13] Xu Xiang, Thomas Viuff, Bernt Leira, Ole Øiseth, "Impact of hydrodynamic interaction between pontoons on global responses of a long floating bridge under wind waves." *ASME 2018 37th International Conference on Ocean, Offshore and Arctic Engineering*. American Society of Mechanical Engineers, 2018.
- [14] Thomas Viuff, Xu Xiang, Bernt Leira, Ole Øiseth, "Code-to-code verification of end-anchored floating bridge global analysis." *ASME 2018 37th International Conference on Ocean, Offshore and Arctic Engineering*. American Society of Mechanical Engineers, 2018.
- [15] Shuai Li, Shixiao Fu, Wei Wei, Torgeir Moan. "A comparison study on the hydroelasticity of two types of floating bridges in inhomogeneous wave conditions." *ASME 2018 37th International Conference on Ocean, Offshore and Arctic Engineering*. American Society of Mechanical Engineers, 2018.
- [16] Statens Vegvesen, SBJ-32-C3-SVV-90-BA-002, Design basis Bjørnafjorden floating bridges, Rev E, 07.03.2017
- [17] Statens Vegvesen, SBJ-31-C4-SVV-26-BA-001, Design basis - Mooring and anchor design, 07.03.2017

- [18] Statens Vegvesen, SBJ-32-C4-SOH-20-RE-001, Wind model-tests Floating Bridge step 1 small scale testing, Rev A, 06.06.2018
- [19] Statens Vegvesen, SBJ-31-C3-MUL-22-RE-114, Bjørnafjorden, straight floating bridge phase 3, Analysis and design (Base Case), Appendix N – Aerodynamics, Rev. 0, 02.06.2017
- [20] Statens Vegvesen, SBJ-31-C3-DNV-62-RE-018, Bjørnafjorden side anchored floating bridge – independent global analyses
- [21] Statens Vegvesen, SBJ-30-C3-NOR-22-TN-001, Technical note: Benchmarking of Orcaflex and 3D float
- [22] Statens Vegvesen, SBJ-31-C3-MUL-22-RE-109, Bjørnafjorden, straight floating bridge phase 3, Analysis and design (Base Case), Appendix I – Design of mooring lines, rev. 0, 02.06.2017
- [23] Arnt G Fredriksen, Mads F. Heiervang, Per N. Larsen, Pål G. Sandnes, Bernt Sørby, Basile Bonnemaire, Anders Nesteby, Øyvind Nedrebø. "Hydrodynamical Aspects of Pontoon Optimization for a Side-Anchored Floating Bridge." ASME 2017 36th International Conference on Ocean, Offshore and Arctic Engineering. American Society of Mechanical Engineers, 2017.
- [24] DNVGL-RP-C201: "Buckling Strength of Plated Structures, October 2010
- [25] Per Norum Larsen, Arnt Fredriksen. "Flytebru over Bjørnafjorden på ferjefri E39." Presentation given in LFCS project workshop in Trondheim 8 March 2018.
- [26] Statens Vegvesen, SBJ-31-C3-DNV-62-RE-017, Bjørnafjorden side anchored floating bridge – independent local analyses

7.3 Sulafjorden Crossing

- [27] Jungao Wang, Etienne Cheynet, Jónas Snæbjörnsson, Jasna B. Jakobsen, "Coupled aerodynamic and hydrodynamic response of a long span bridge suspended from floating towers." *Journal of Wind Engineering and Industrial Aerodynamics* 177 (2018): 19-31.
- [28] Jungao Wang, Lin Li, Jasna B. Jakobsen, Sverre K. Haver, "Metocean Conditions in a Norwegian Fjord", ASME 2018 37th International Conference on Ocean, Offshore and Arctic Engineering. American Society of Mechanical Engineers, 2018

7.4 Lysefjorden

- [29] Jungao Wang, Etienne Cheynet, Jasna B. Jakobsen, Jónas Snæbjörnsson, "Time-Domain Analysis of Wind-Induced Response of a Suspension Bridge in Comparison With the Full-Scale Measurements." ASME 2017 36th International Conference on Ocean, Offshore and Arctic Engineering. American Society of Mechanical Engineers, 2017.
- [30] Etienne Cheynet, Jasna Bogunović Jakobsen, and Jónas Snæbjörnsson. "Buffeting response of a suspension bridge in complex terrain." *Engineering Structures* 128 (2016): 474-487.

7.5 Other bridges

- [31] Knut Andreas Kvåle, Ragnar Sigbjörnsson, and Ole Øiseth. "Modelling the stochastic dynamic behaviour of a pontoon bridge: A case study." *Computers & Structures* 165 (2016): 123-135.
- [32] Aksel Fenerci, and Ole Øiseth. "The Hardanger Bridge monitoring project: Long-term monitoring results and implications on bridge design." *Procedia engineering* 199 (2017): 3115-3120.

- [33] Aksel Fenerci, and Ole Øiseth. "Measured buffeting response of a long-span suspension bridge compared with numerical predictions based on design wind spectra." *Journal of Structural Engineering* 143.9 (2017): 04017131.
- [34] Knut Andreas Kvåle, "Dynamic behaviour of floating bridges exposed to wave excitation", 2017, PhD Thesis
- [35] Luca Salvatori, and Paolo Spinelli. "Effects of structural nonlinearity and along-span wind coherence on suspension bridge aerodynamics: Some numerical simulation results." *Journal of Wind Engineering and Industrial Aerodynamics* 94.5 (2006): 415-430.
- [36] FEDA-F1 and FEDA-F2: Theory Manual, SINTEF Report, STF71 F88023, Trondheim, 1988.
- [37] Giske, F.-I. G., Leira, B. J. and Øiseth, O. (2017a): 'Long-term stochastic extreme response analysis of floating bridges'. *Procedia Engineering* 199, pp. 1175–1180. doi:10.1016/j.proeng.2017.09.305.
- [38] Giske, F.-I. G., Leira, B. J. and Øiseth, O. (2017b): 'Long-term extreme response analysis of marine structures using inverse SORM'. *Proceedings of the ASME 2017 36th International Conference on Ocean, Offshore and Arctic Engineering*.
- [39] O. Øiseth: "A note on long-term distribution of wind induced load effects with applications to structures with high natural periods", NTNU 2017

Appendix A Bridge concepts; some examples

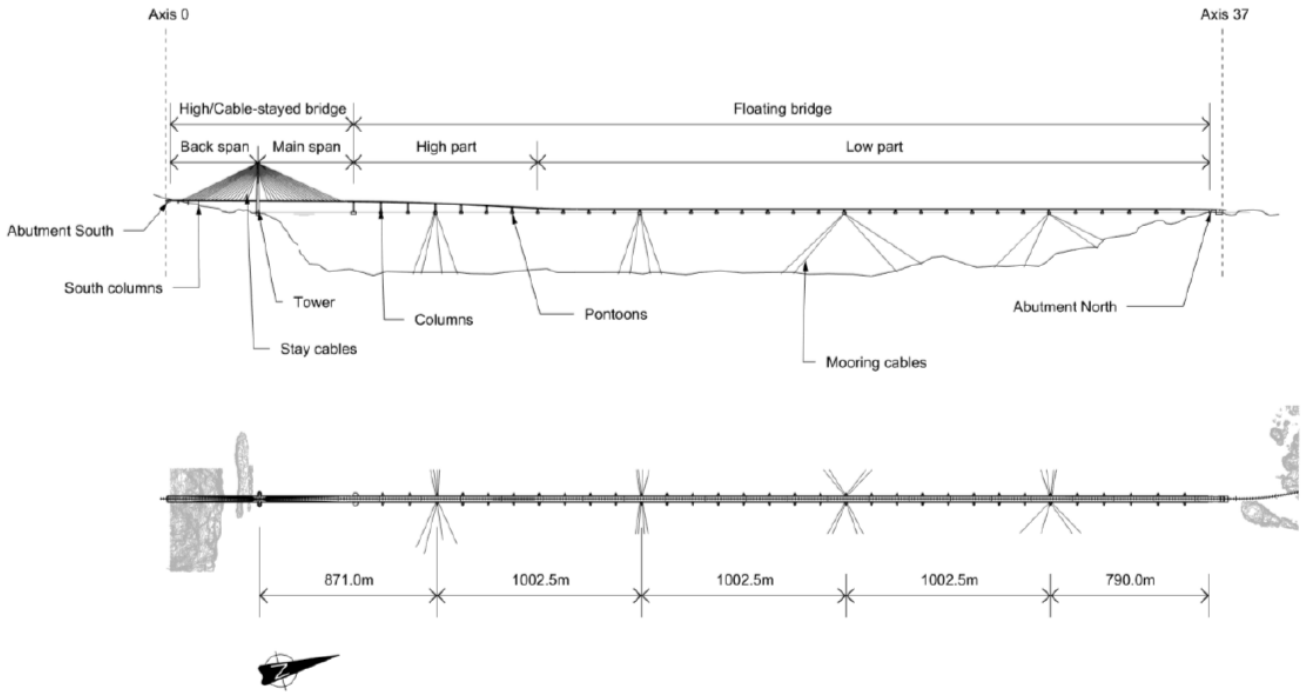


Figure 25 Bjørnafjorden side-anchored bridge [5]

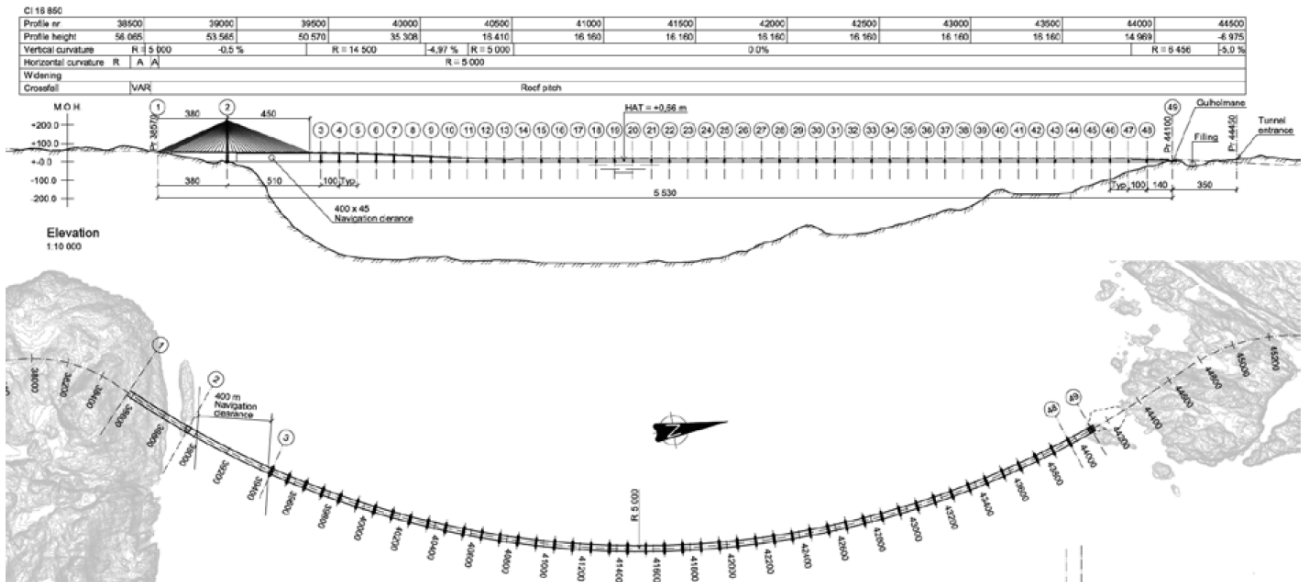


Figure 26 Bjørnafjorden end-anchored bridge [6]

